FISSION TRACK CONSTRAINTS ON EXHUMATION AND EXTENSIONAL FAULTING IN SOUTHWEST NEVADA AND EASTERN CALIFORNIA, U.S.A.

Prepared for

U.S. Nuclear Regulatory Commission
Contract NRC–02–07–006

Prepared by

David A. Ferrill,[1] Alan P. Morris,[1]
John A. Stamatakos,[2] Deborah J. Waiting,[2]
Raymond A. Donelick,[3] Ann E. Blythe[4]

[1]Department of Earth, Material, and Planetary Sciences
Southwest Research Institute®
San Antonio, Texas

[2]Center for Nuclear Waste Regulatory Analyses
San Antonio, Texas

[3]Apatite to Zircon, Inc.
Viola, Idaho

[4]Department of Geology
Occidental College
Los Angeles, California

September 2011

ABSTRACT

Eastern California and southwestern Nevada is an area of Tertiary and Quaternary extensional and dextral transtensional deformation. We use zircon and apatite fission-track thermochronology to study the distribution and timing of tectonic exhumation resulting from extensional and transtensional detachment faulting in this area. Samples were collected from outcrops around Yucca Flat and Frenchman Flat, the Striped Hills, Mount Stirling, Resting Spring Range, Bare Mountain, Bullfrog Hills, and the eastern margin of the Funeral Mountains. To constrain timing of exhumation associated with crustal-scale normal faulting, sampling efforts were focused on Paleozoic and Precambrian clastic sedimentary and metasedimentary rocks of the Stirling Quartzite, Wood Canyon Formation, Zabriskie Quartzite, Eureka Quartzite, and Eleana Formation. Sixty-nine new apatite and zircon fission-track cooling ages from 50 samples, analyzed in conjunction with published fission-track data from the region, indicate a distinct population of young (Miocene) fission-track ages and a population of irregularly distributed older (pre-Miocene) fission-track ages. Miocene (young population) fission track ages young westwards—indicating westward migration of the cooling front, consistent with well-documented Miocene extension of the Basin and Range. The younging pattern is also consistent with west-northwest displacement of the hanging wall of a crustal scale extensional fault system and consequent progressive footwall exhumation. The active trailing edge of the hanging wall of this system generally coincides with Death Valley. Migration rates of the cooling front in the footwall of this system are on the order of 10–11 mm/yr [0.39–0.43 in]. Based on the distribution of the Miocene fission-track ages, we interpret that the crustal faults that defined the eastern edge of the detachment system originated as separate normal faults that were linked by the formation of a transfer fault, similar in geometry to the Panamint Valley–Hunter Mountain–Saline Valley fault system. The complex hanging wall of this crustal detachment system includes high mountain ranges, including the Panamint, Cottonwood, Argus, Inyo, White, and Last Chance Ranges, separated by active graben and half-graben basins, including the Panamint, Saline, Eureka, Deep Springs, and Owens Valleys. Extrapolation of apatite fission-track closure ages from two transects across the eastern margin of the Death Valley region suggests that exhumation along the eastern margin of the system continues beneath Death Valley today.

TABLE OF CONTENTS

Section Page

ABSTRACT ii
FIGURES iv
TABLES v
ACKNOWLEDGMENTS vi

1 INTRODUCTION 1-1

2 FISSION-TRACK METHODS 2-1

3 SAMPLING 3-1

4 APATITE FISSION-TRACK THERMOCHRONOLOGY RESULTS 4-1

5 ZIRCON FISSION-TRACK THERMOCHRONOLOGY RESULTS 5-1

6 DISCUSSION 6-1

7 CONCLUSIONS 7-1

8 REFERENCES 8-1

APPENDIX A—APATITE FISSION-TRACK THERMOCHRONOLOGY
APPENDX B—ZIRCON FISSION-TRACK THERMOCHRONOLOGY

FIGURES

Figure Page

1-1 Digital Shaded Relief Model of the Western Basin and Range, Showing Location of Detailed Study Area Within the Walker Lane Belt. 1-2

3-1 Simplified Geologic Map (Based on Workman, et al., 2002) of the Study Area Showing Sample Locations in Their Geologic Context 3-2

3-2 Generalized Chart Showing Stratigraphic Position of Paleozoic Units Exposed at Bare Mountain, Nevada; Death Valley, California; and the Surrounding Area 3-3

4-1 Shaded Relief Digital Elevation Model of Southern Nevada and California Showing Locations of Apatite Fission-Track Sample Locations and Ages Sampled for This Study 4-7

5-1 Shaded Relief Digital Elevation Model of Southern Nevada and California Showing Locations of Zircon Fission-Track Sample Locations and Ages Sampled for This Study 5-3

5-2 Age Versus Count Plots of Zircon and Apatite Cooling Ages Based on Data in Tables 4-1 and 5-1. 5-4

6-1 Models of Faulting, Exhumation, and Isostatic Adjustment Illustrating Unroofing of Rocks With Reset Apatite and Zircon Ages 6-2

6-2 (A) Digital Shaded Relief Map Illustrating the Interpreted Position of the Breakaway Fault, Interpretation of Domains With Respect to Detachment System, and Location of Transects in (B) and (C) 6-3

TABLES

Table Page

4-1 Apatite Fission-Track Data 4-2

5-1 Zircon Fission-Track Data 5-2

ACKNOWLEDGMENTS

This paper was prepared as a result of work performed at the Center for Nuclear Waste Regulatory Analyses (CNWRA®) for the U.S. Nuclear Regulatory Commission (USNRC) under contract numbers NRC–02–93–005, NRC–02–97–009, and NRC–02–02–012. This work was initiated on behalf of the USNRC Office of Nuclear Regulatory Research as part of the Tectonic Processes of the Central Basin and Range research project and continued on behalf of the Office of Nuclear Material Safety and Safeguards. This report is an independent product of the CNWRA and does not necessarily reflect the views or regulatory position of the USNRC.

The authors thank Steven Young, Lawrence McKague, Kathy Spivey, Bret Rahe, Sid Jones, and Don Cederquist for their assistance and Tom John for allowing us to sample in the Barrick Bullfrog Mine. We also thank Ron McGinnis and English Pearcy for their review comments, Arturo Ramos for secretarial support, and Lauren Mulverhill for editorial review.

QUALITY OF DATA, ANALYSES, AND CODE DEVELOPMENT DATA

DATA: All CNWRA-generated data contained in this report meet quality assurance requirements described in the Geosciences and Engineering Division Quality Assurance Manual. Sources of other data should be consulted for determining the level of quality of those data.

ANALYSES AND CODES: No scientific and engineering software was used in the analyses contained in this report.

1 INTRODUCTION

Yucca Mountain is located in the western Basin and Range Province, an area of active tectonic deformation. Tectonic models and interpretations of the timing and rate of tectonic deformation in the Yucca Mountain region have varied widely (e.g., McKague, et al., 2010). In 1993, staff of the Center for Nuclear Waste Regulatory Analyses (CNWRA®) began sampling for fission-track dating to better constrain timing and rate of crustal thinning by normal faults in the vicinity of Yucca Mountain. The focus was to reduce key technical uncertainties for fault-related processes that would need to be assessed for regulatory compliance evaluations with respect to long-term performance of a potential high-level radioactive waste repository at Yucca Mountain. Early analyses focused on Bare Mountain (the mountain range west of Yucca Mountain across Crater Flat Basin) and were presented by Ferrill, et al. (1995). Sampling was later expanded to provide a broader regional context and tie in other published fission-track data sets. In this report, we present the entire fission-track data set collected from the Yucca Mountain region by CNWRA, include other published data from the region, and present a summary of these results and constraints provided by the data on the timing and rate of lower crustal exhumation in the Yucca Mountain region.

Oblique motion between the Pacific and North American plates produces a transtensional tectonic regime in the western Basin and Range Province of eastern California and southern Nevada (Harland, 1971; Atwater, 1970; Frisch, et al., 2011). Active deformation in this region is manifested by an interconnected network of large-scale north-south striking normal faults and northwest-trending strike-slip faults, an area Stewart (1988) referred to as the Walker Lane Belt (Figure 1-1). Although there is debate about the total amount of extension in the region (e.g., Serpa and Pavlis, 1996) and the details of fault block definition and displacement style (e.g., Snow and Wernicke, 2000), there is consensus that rapid and continuing displacement on this network of basin-controlling faults is producing pull-apart basins linked by strike-slip faults (Zoback, et al., 1981; Burchfiel, et al., 1987; MIT 1985 Field Geophysics Course and Biehler, 1987; Dixon, et al., 2000, 1995; Rahe, et al., 1998; Sims, et al., 1999; McQuarrie and Wernicke, 2005).

Slow rates of erosion and sedimentation, combined with high slip rates, have generated starved basins (where rate of subsidence exceeds rate of sedimentation) with several kilometers of structural and topographic relief. Most of these active basins have developed since the late Miocene (e.g., MIT 1985 Field Geophysics Course and Biehler, 1987; Snow and Wernicke, 2000), although there is also evidence of Eocene, Oligocene, and early Miocene basin development in the region (Axen, et al., 1993; Ridgway, et al., 2011). Along the eastern margin of this region of active and rapid basin formation is the Death Valley–Furnace Creek fault system. East of this fault system, displacement on normal faults initiated in the Miocene and has exhumed rocks from depths of 10 to 15 km [6 to 9 mi] (Hodges, et al., 1987; Hoisch and Simpson, 1993; Hoisch, et al., 1997; Holm and Dokka, 1993, 1991). Exhumation of deep footwall rocks during deformation led to progressively more brittle overprinting of earlier formed ductile deformation features at the northern end of the Panamint Range (Hodges, et al., 1989), the Black Mountains (Cowan, et al., 2003; Miller and Pavlis, 2005; Hayman, 2006), and the Funeral Mountains (Hoisch and Simpson, 1993). Isostasy is presumed to have produced uplift of footwalls relative to hanging walls, placing rocks from 10- to 15-km [6- to 9-mi] depths at the same elevation as uppermost crustal rocks (e.g., Asmerom, et al., 1990; Wernicke, 1992). Analog modeling that simulates brittle deformation of the upper crust above more ductile lower crustal material has reproduced many of the key structural elements seen in the region (Brun, et al., 1994).

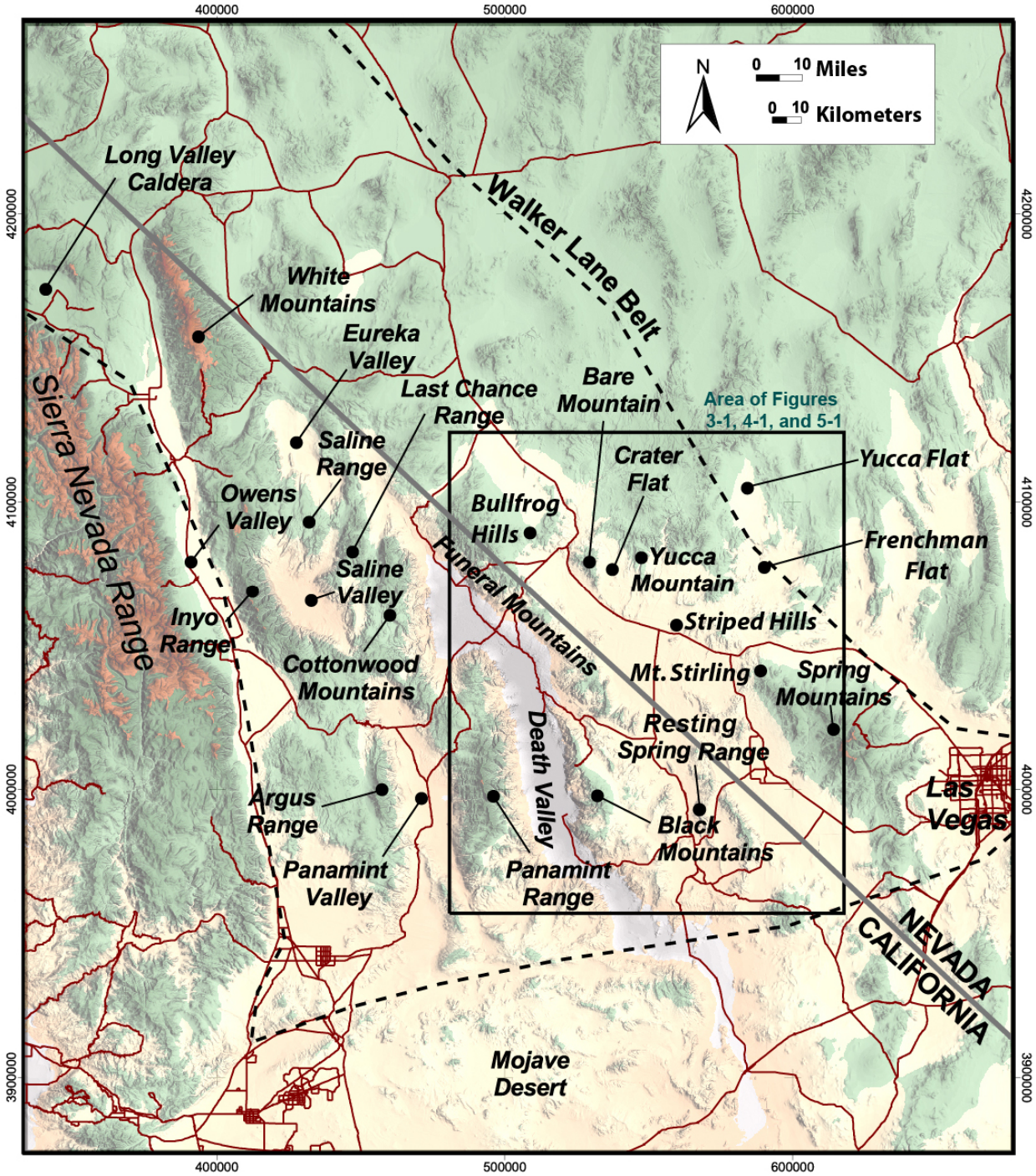

Figure 1-1. Digital Shaded Relief Model of the Western Basin and Range, Showing Location of Detailed Study Area Within the Walker Lane Belt. Coordinate Projection Is Universal Transverse Mercator, Zone 11, NAD 27.

The purpose of this report is to summarize fission track cooling ages and related distribution and timing of fault-related exhumation of crustal rocks in the vicinity of Yucca Mountain, Nevada. These results provide important constraints on tectonic models of the Yucca Mountain area. We use fission-track ages from apatite and zircon as a basis for interpreting the distribution and timing of exhumation for pre-Miocene rocks in southwest Nevada and eastern California. We present 69 new apatite and zircon fission-track ages collected from Paleozoic and Precambrian rocks throughout the study area. The fission-track ages indicate exhumation ages of the sample host rocks as these rocks cooled through the fission-track closure temperatures of apatite and zircon. Our results define an area of Miocene crustal extension exhumed by normal faulting. Spatial distribution of the fission-track ages is also used to infer the original configuration of crustal faults that define the detachment system.

2 FISSION-TRACK METHODS

Fission tracks are linear damage zones caused by spontaneous fission of uranium atoms in U-bearing minerals such as apatite and zircon. U-238 decay occurs at a known rate unaffected by temperature or pressure, and the number of fission tracks per unit area of crystal in conjunction with the uranium concentration gives a measure of the time since track accumulation began (Wagner and Van den Haute, 1992). Fission tracks are not permanent features of a crystal and are subject to healing or annealing if the crystal is heated above its closure temperature for a period of ~10^6 years (Tagami and O'Sullivan, 2005). While at temperatures above the closure temperature, rates of fission-track formation within the crystal are balanced by rates of annealing and there is no net fission-track accumulation. Below the closure temperature, however, annealing is inhibited and fission tracks accumulate within the crystal. Thus a fission-track age is a measure of the time elapsed since the latest cooling of the crystal through its closure temperature. If the rock in which the mineral sample resides had been buried to depths at which the ambient temperature was greater than the fission-track closure temperature for that mineral, then the fission-track age also represents the time at which the rock was exhumed by erosion, extensional faulting, or a combination of these processes. Typical long-term (geological) cooling rates for crustal rocks exhumed by these processes would be on the order of 10–100°C/my [18–180°F/my].

For fast-annealing, typical Ca-F-rich apatite, the closure temperature is estimated to be 130–146 °C [266–295 °F] for cooling rates of 10–100 °C/my [18–180 °F/my] (Ketcham, et al., 1999). For slow annealing, oftentimes Cl-rich and possibly Mn-, Fe-, and/or REE-rich apatite, the closure temperature is estimated to be as high as 172 °C [342 °F] for cooling rates of 10–100 °C/my [18–180 °F/my] (Ketcham, et al., 1999). Fast-annealing apatites are typically less soluble in the nitric acid used to reveal the tracks for observation and measurement. The mean diameter of fission-track etch pits (Dpar) on the apatite surface being studied is usually less than 2 µm [0.000079 in] for the etching conditions used in this study (e.g., Carlson, et al., 1999; Donelick, et al., 2005). As discussed in Appendix A, the apatite grains in this study were dominantly fluorine-rich, as indicated by their small fission-track etch pit diameters. Assuming an average surface temperature of 15°C [59°F] and a constant geothermal gradient of 30 °C/km [87 °F/mi] (Ferrill, et al., 1995; 1996a), an apatite closure temperature of 138 °C [280 °F] would equate to a depth of approximately 4.1 km [2.55 mi].

Zircon has a higher estimated closure temperature. Early estimates of zircon closure temperatures ranged from 175 ± 25 °C [347 ± 45 °F] (Harrison and McDougall, 1980) to 230 ± 5 °C [446 ± 9 °F] for cooling rates of 10 to 30 °C/my [18 to 54 °F/my] Brandon and Vance (1992) modeled from annealing data of Zaun and Wagner (1985) and Tagami, et al. (1990) and closure temperature equations of Dodson (1979, 1973). More recently, borehole data from the Vienna basin (Tagami, et al., 1995), laboratory annealing data (Yamada, et al., 1995), and natural annealing data from the contact metamorphic aureole around a granite pluton (Tagami and Shimada, 1996) have suggested a significantly higher temperature range for the zircon annealing zone, ~230 to ~330 °C [446 to 626 °F], and a zircon closure temperature of 250 °C [482 °F] for cooling rates of 10–100 °C/my [18–180 °F/my] (Tagami and Shimada, 1996; Foster, et al., 1993). Assuming an average surface temperature of 15 °C [59 °F] and a constant geothermal gradient of 30 °C/km [87 °F/mi] (Ferrill, et al., 1995; 1996a), a zircon closure temperature of 250°C [482 °F] would equate to a depth of approximately 7.8 km [4.85 mi].

3 SAMPLING

Samples were collected from outcrops around Yucca Flat and Frenchman Flat (on the Nevada Test Site), the Striped Hills, Mount Stirling, Resting Spring Range, Bare Mountain (Spivey, et al., 1995; Ferrill, et al., 1996a), Bullfrog Hills, and the eastern margin of the Funeral Mountains (Figures 1-1 and 3-1). Sampling sites were selected to expand upon previous fission-track results that concentrated on mountain ranges along the eastern margin of Death Valley, the Bullfrog Hills, and the northwest corner of Bare Mountain. To constrain timing of exhumation associated with crustal-scale normal faulting, we focused our sampling efforts on Paleozoic and Precambrian clastic sedimentary and metasedimentary rocks of the Stirling Quartzite, Wood Canyon Formation, Zabriskie Quartzite, Eureka Quartzite, and Eleana Formation (see Figure 3-2 for stratigraphic positions and data tables in Sections 4 and 5 for details on sampled rock types).

In a few cases, we sampled younger igneous rocks to provide an independent check of dating results and additional geochronologic constraints. For these purposes, samples were collected from Cretaceous granite and Tertiary diorite and latite dikes at Bare Mountain, Mesozoic monzogranite of the Climax Stock (northwest Yucca Flat), and Rainier Mesa tuff from the Bullfrog Hills. In total, 50 new samples were collected for dating. Apatite and zircon mineral separates were isolated from each sample following procedures outlined in Dumitru (1999) using standard gravimetric and magnetic mineral separation techniques. The apatite mineral separates consist of fluorine-rich apatite. Apatite fission-track ages were measured at Apatite to Zircon, Inc. by Raymond A. Donelick (analyst RAD; see Appendix A) using the external detector method (e.g., Gleadow, 1981). Zircon grains from 16 samples were analyzed using zircon fission-track thermochronology techniques (e.g., Wagner and Van den Haute, 1992). Eleven of the zircon fission-track age analyses were performed at University of California at Santa Barbara by Ann E. Blythe (analyst AEB), and 5 were performed at Apatite to Zircon, Inc. (analyst RAD; see Appendix B). All analyses were performed using the external detector method (e.g., Gleadow, 1981). Fission track analyses are detailed in Appendices A and B.

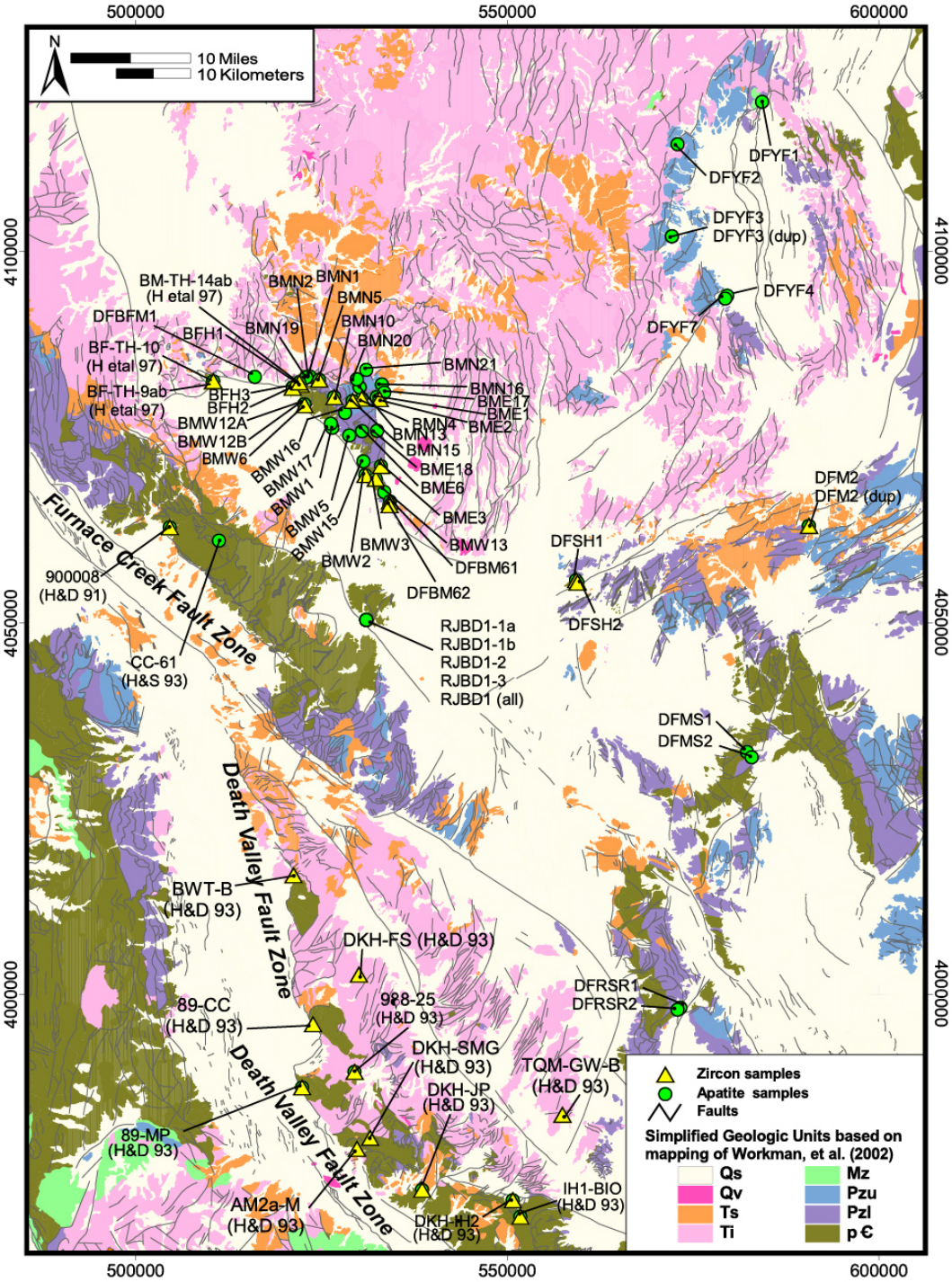

Figure 3-1. Simplified Geologic Map (Based on Workman, et al., 2002) of the Study Area Showing Sample Locations in Their Geologic Context. Qs = Quaternary Sedimentary Units, Qv = Quaternary Volcanic Units, Ts = Tertiary Sedimentary Units, Ti = Tertiary Igneous Units, Mz = Mesozoic Units, Pzu = Upper Paleozoic Units, Pzl = Lower Paleozoic Units, pC = Precambrian Units. H etal 97 = Hoisch, et al., 1997; H&S 93 = Hoisch and Simpson, 1993; H&D 93 = Holm and Dokka, 1993.

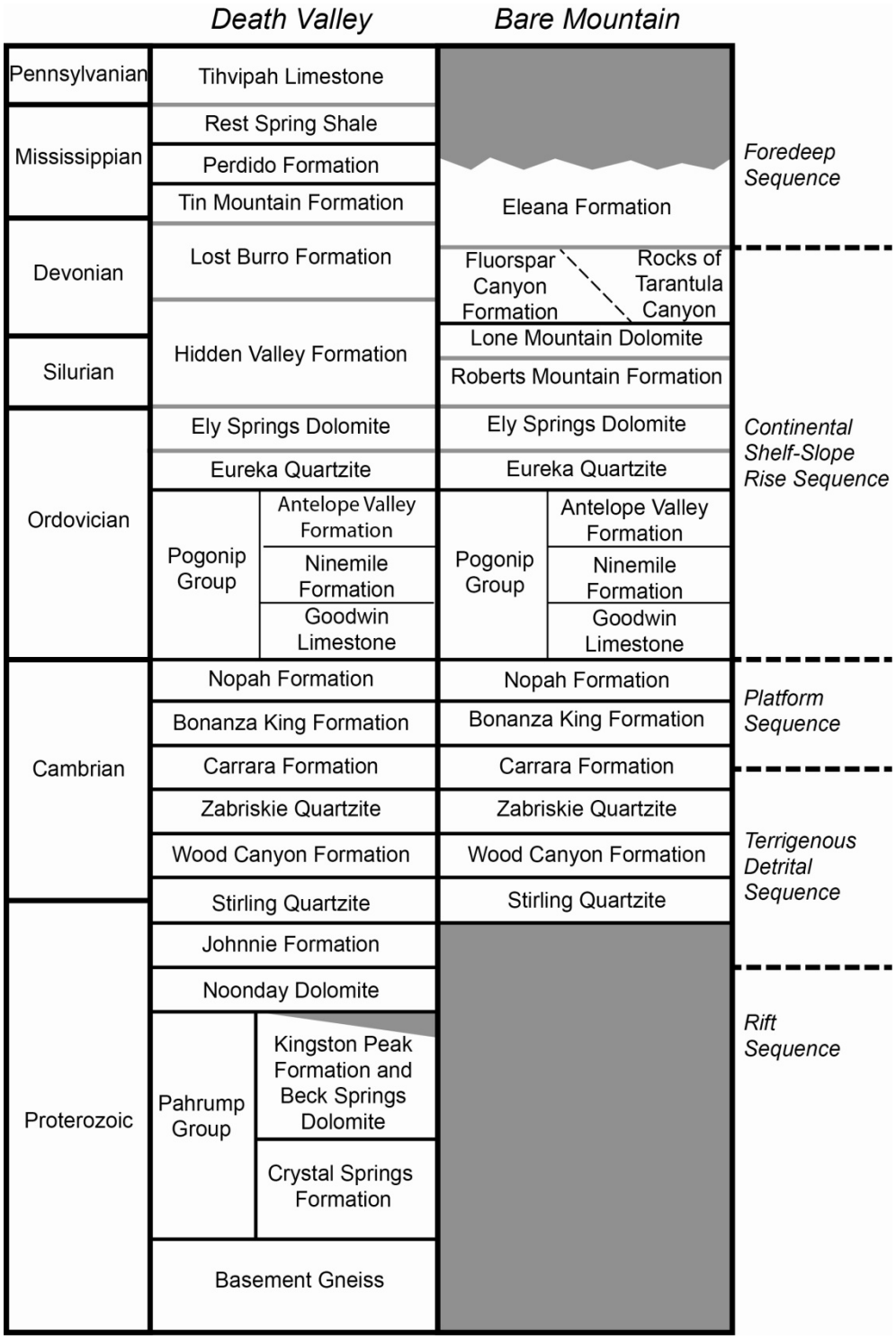

Figure 3-2. Generalized Chart Showing Stratigraphic Position of Paleozoic Units Exposed at Bare Mountain, Nevada; Death Valley, California; and the Surrounding Area (After Poole, 1974; Poole, et al., 1992; and Monsen, et al., 1992). Gray Areas Show Gaps in the Geologic Record Due to Nondeposition, Faulting, or Erosion.

4 APATITE FISSION-TRACK THERMOCHRONOLOGY RESULTS

Except for the Miocene silicic porphyry dikes at Bare Mountain (apatite fission-track ages 10.9 to 16.0 Ma) (Monsen, et al., 1992), the Rainier Mesa Tuff from the Bullfrog mine (apatite fission-track age 21.3 Ma), and the Climax stock (apatite fission-track age 76 Ma) (Naeser and Maldonado, 1981) in northern Yucca Flat (Figure 1-1), all apatite fission-track ages reported here (Table 4-1) are significantly younger than the host rocks. Of the 53 ages reported here (including 2 duplicates and 1 combined), 50 exhibit Dpar values less than or equal to 2 μm [0.000079 in], indicating that the apatites can be treated as fast annealing for interpretation purposes. In general, fission-track ages that are younger than the host rock indicate heating above the temperatures required for total fission-track annealing after deposition or crystallization of the host rocks. Thus, the ages are not inherited (e.g., from rocks of a previously eroded terrain); rather, they represent cooling of the host rocks through the fluorine-rich apatite closure temperature, presumably during exhumation. In addition to our 53 new ages, we include 10 published ages from the Black Mountains (Holm and Dokka, 1993), the Funeral Mountains (Holm and Dokka, 1991; Hoisch and Simpson, 1993), and the Bullfrog Hills and northwest corner of Bare Mountain (Hoisch, et al., 1997).

Apatite fission-track ages fall into a population of diverse pre-Miocene ages and a population of Miocene and younger ages (Figure 4-1). Pre-Miocene ages generally lie to the east of Miocene ages at a given latitude in the study area and range from 25–115 Ma. To assess spatial variation of the Miocene and younger ages, we subdivided these ages into three groups: (i) early Miocene (16.6–23.7 Ma), (ii) middle Miocene (11.2–16.6 Ma), and (iii) late Miocene (5.3–11.2 Ma) and younger (Figure 4-1). The youngest ages are found along the eastern margin of Death Valley in the Funeral Mountains and Black Mountains. Miocene cooling ages generally young to the west or northwest. The Funeral Mountains and Bare Mountain include ages belonging to both the Miocene and pre-Miocene populations, which allows us to delineate these age transitions in bedrock within these ranges.

Table 4-1. Apatite Fission-Track Data

Site	Rock Type	Easting	Northing	ρ_s	Ns	ρi	Ni	ρd	Nd	Grains	Q	χ2	Dpar	Pooled Age	Mean Age	NT	Mean Length	σ	U
Analyst RAD																			
BFH1	Wood Canyon Formation (schist)	522200	4082050	0.116	88	2.361	1792	5.238	4105	25	0.998	P	1.60	**14.6 ± 1.7**	14.7 ± 1.2	75	14.26 ± 0.19	1.61	23
BFH2	Wood Canyon Formation (schist)	521130	4081680	0.127	96	3.390	2560	5.249	4105	25	0.210	P	1.58	**11.2 ± 1.2**	9.9 ± 1.5	101	14.12 ± 0.17	1.66	59
BFH3	Stirling Quartzite (D member)	521130	4081660	0.095	66	2.810	1951	5.259	4105	22	0.129	P	1.66	**10.1 ± 1.3**	13.0 ± 2.4	51	13.79 ± 0.26	1.87	29
BMN1	Granite	523380	4083170	0.035	19	0.909	489	5.158	4105	25	0.729	P	1.61	**1.4 ± 2.7**	11.9 ± 3.2	51	14.05 ± 0.15	1.04	9
BMN2	Diorite Dike	522950	4083130	0.113	15	2.151	285	5.324	4105	18	0.945	P	1.65	**15.9 ± 4.2**	14.7 ± 5.1	33	13.91 ± 0.30	1.70	16
BMN4	Zabriskie Quartzite	530360	4080190	0.270	81	5.205	1559	5.335	4105	25	0.035	F	1.79	15.8 ± 1.9	**20.2 ± 4.4**	30	13.47 ± 0.51	2.75	57
BMN5	Zabriskie Quartzite	524640	4082730	0.049	28	1.311	749	5.345	4105	25	0.788	P	1.49	**11.4 ± 2.2**	13.4 ± 4.0	14	13.53 ± 0.51	1.84	15
BMN10	Zabriskie Quartzite	526671	4080373	0.219	31	8.421	1191	5.356	4105	13	0.177	P	1.65	**7.9 ± 1.5**	7.5 ± 2.9	14	12.51 ± 1.14	4.10	72
BMN13	Eureka Quartzite	530130	4081726	0.139	62	3.037	1351	5.086	4236	22	0.575	P	1.69	**13.3 ± 1.8**	13.6 ± 3.3	12	13.50 ± 0.59	1.94	34
BMN15	Zabriskie Quartzite	529163	4079903	0.279	58	5.471	1138	5.074	4236	15	0.788	P	1.73	**14.7 ± 2.0**	15.8 ± 2.7	18	14.09 ± 0.35	1.46	56
BMN16	Quartz Latite Dike	533093	4082128	0.050	19	0.925	353	4.578	4116	24	0.706	P	1.70	**14.0 ± 3.3**	10.7 ± 3.0	47	13.99 ± 0.28	1.88	10
BMN19	Wood Canyon Formation (quartzite; lower member unit D)	522933	4083039	0.059	15	1.523	384	5.057	4236	23	0.207	P	1.61	**11.2 ± 3.0**	7.8 ± 3.4	83	13.63 ± 0.21	1.89	16
BMN20	Eureka Quartzite	529724	4082811	0.331	21	5.556	352	5.003	4236	9	0.774	P	2.16	**17.0 ± 3.8**	12.8 ± 5.2	12	14.13 ± 0.48	1.73	46
BMN21	Eureka Quartzite	531044	4084040	0.104	1	6.042	58	4.995	4236	1	n.a.	n.a.	1.55	**4.9 ±4.9**	4.9	3	14.17 ± 0.75	1.06	56
BME1	Eleana Formation (conglomerate)	532430	4080400	0.136	38	3.528	989	5.270	4105	25	0.143	P	1.61	**11.5 ± 1.9**	12.9 ± 4.5	12	13.72 ± 0.44	1.46	32

Table 4-1. Apatite Fission-Track Data (continued)

Site	Rock Type	Easting	Northing	ρ_s	Ns	ρi	Ni	ρd	Nd	Grains	Q	χ2	Dpar	Pooled Age	Mean Age	NT	Mean Length	σ	U
BME2	Quartz Latite Dike	532780	4080120	0.035	15	0.857	368	5.287	4105	24	0.462	P	1.76	**12.3 ± 3.2**	11.6 ± 3.7	51	13.51 ± 0.35	2.51	8
BME3	Wood Canyon Formation (quartzite)	533000	4071100	0.039	5	0.891	114	5.308	4105	9	0.900	P	1.50	**13.2 ± 6.1**	7.4 ± 6.0	11	12.26 ± 0.88	2.77	8
BME6	Quartz Latite Dike	530456	4075819	0.038	27	0.641	451	4.576	4116	23	0.766	P	2.37	**15.6 ± 3.1**	16.0 ± 3.0	54	14.83 ± 0.21	1.50	7
BME17	Quartz Latite Dike	533452	4081028	0.143	12	2.684	225	5.024	4236	11	0.594	P	1.57	**15.2 ± 4.5**	15.4 ± 8.9	0	n.a.	n.a.	29
BME18	Stirling Quartzite (E member)	532490	4075863	0.250	79	5.032	1591	5.011	4236	24	0.930	P	1.67	**14.1 ± 1.7**	15.7 ± 1.8	30	13.64 ± 0.30	1.61	57
BMW1	Stirling Quartzite (schist; C member)	526475	4076240	0.026	11	0.440	189	5.173	4105	23	0.321	P	1.50	**17.1 ± 5.3**	19.0 ± 6.8	8	12.14 ± 1.04	2.76	5
BMW2	Wood Canyon Formation (quartzite; lower member, unit A)	530880	4069920	0.027	11	0.707	286	5.190	4105	20	0.535	P	1.60	**11.3 ± 3.5**	16.1 ± 7.4	26	12.75 ± 0.60	3.02	11
BMW3	Stirling Quartzite (D member)	532300	4069380	0.161	92	3.563	2032	5.206	4105	24	0.575	P	1.57	**13.4 ± 1.5**	20.3 ± 3.3	26	13.00 ± 0.40	2.00	48
BMW5	Zabriskie Quartzite	528730	4075260	0.057	14	1.643	406	5.212	4105	22	0.238	P	1.60	**10.2 ± 2.8**	12.3 ± 5.8	8	12.70 ± 0.64	1.69	14
BMW6	Stirling Quartzite (D member)	522690	4079300	0.072	33	1.630	752	5.045	4236	25	0.956	P	1.88	**12.6 ± 2.3**	11.3 ± 2.1	104	13.74 ± 0.18	1.81	17
BMW12A	Stirling Quartzite (D member)	522677	4079457	0.094	19	1.830	369	5.367	4105	20	0.899	P	1.66	**15.7 ± 3.7**	18.1 ± 3.7	48	14.01 ± 0.26	1.76	17
BMW12B	Diorite Dike	522677	4079457	0.084	12	2.463	350	5.036	4236	14	0.575	P	1.56	**9.8 ± 2.9**	10.9 ± 4.0	0	n.a.	n.a.	22
BMW13	Stirling Quartzite (A member)	533455	4067605	0.013	2	0.800	125	4.987	4236	8	0.645	P	1.58	**4.5 ± 3.2**	4.3 ± 3.8	12	12.30 ± 0.67	2.24	8
BMW15	Stirling Quartzite (A member)	530632	4071735	0.104	19	2.530	463	4.970	4236	18	0.840	P	1.75	**11.6 ± 2.7**	11.4 ± 2.8	2	0.49 ± 1.10	1.10	30

Table 4-1. Apatite Fission-Track Data (continued)

Site	Rock Type	Easting	Northing	ρ_s	Ns	ρi	Ni	ρd	Nd	Grains	Q	χ2	Dpar	Pooled Age	Mean Age	NT	Mean Length	σ	U
BMW16	Eureka Quartzite	528139	4078281	0.938	15	28.750	460	4.962	4236	2	0.343	P	1.68	**9.2 ± 2.4**	16.2 ± 10.4	1	12.29	n.a.	213
BMW17	Stirling Quartzite (schist; C member)	526251	4076808	0.110	11	3.576	357	4.953	4236	12	0.829	P	1.54	**8.7 ± 2.7**	5.7 ± 2.8	1	12.49	n.a.	32
DFBM61	Zabriskie Quartzite	534210	4066361	0.644	134	3.663	762	4.585	4116	24	0.126	P	1.83	**45.7 ± 4.5**	40.7 ± 6.5	27	10.56 ± 0.70	3.54	76
DFBM62	Zabriskie Quartzite	534135	4065850	1.258	128	6.899	702	4.587	4116	10	0.824	P	1.79	**47.4 ± 4.8**	49.1 ± 8.0	30	11.11 ± 0.51	2.75	71
DFSH1	Zabriskie Quartzite	559253	4055732	0.588	164	2.476	691	4.945	4236	14	0.038	F	1.99	66.4 ± 6.1	**65.9 ± 9.8**	43	11.83 ± 0.34	2.19	32
DFSH2	Wood Canyon Formation (quartzite)	559409	4055393	0.768	290	2.781	1050	4.937	4236	25	0.320	P	1.97	**77.1 ± 5.6**	87.9 ± 8.3	148	11.47 ± 0.20	2.37	32
DFBFM1	Rainier Mesa Tuff	516010	4083130	0.047	4	1.140	97	4.583	4116	13	0.170	P	1.76	**10.7 ± 5.5**	21.3 ± 12.0	1	12.48	n.a.	13
DFM2	Eureka Quartzite	590572	4063062	0.938	239	2.120	540	4.589	4116	25	0.292	P	1.89	**115 ± 10**	128 ± 14	124	12.63 ± 0.17	1.90	37
DFM2 (dup)	Eureka Quartzite	590572	4063062	2.128	301	5.253	743	4.612	4116	22		P	2.03	**105 ± 8**	102 ± 11	49	12.88 ± 0.27	1.88	64
DFMS1	Stirling Quartzite	582236	4032599	1.454	388	5.141	1372	4.592	4116	24	0.679	P	1.78	**73.5 ± 4.8**	78.5 ± 5.6	112	12.57 ± 0.18	1.89	102
DFMS2	Stirling Quartzite	582845	4031897	0.915	339	2.968	1100	4.594	4116	23	0.376	P	1.84	**80.1 ± 5.5**	83.9 ± 9.8	107	12.91 ± 0.16	1.67	44
DFRSR1	Stirling Quartzite	573252	3998158	2.146	239	5.532	616	4.596	4116	16	0.511	P	1.89	**101 ± 8**	99.4 ± 9.3	49	13.72 ± 0.27	1.89	76
DFRSR2	Stirling Quartzite	572878	3997924	1.478	123	4.303	358	4.598	4116	16	0.094	P	1.75	**89.3 ± 9.7**	106 ± 19	47	13.07 ± 0.32	2.15	73
DFYF1	Monzogranite (Climax)	584257	4120177	0.371	336	1.246	1129	4.600	4116	25	0.597	P	1.77	**77.4 ± 5.3**	76.0 ± 5.2	127	13.25 ± 0.12	1.37	13
DFYF2	Eleana Formation (cng.)	572878	4114429	0.266	40	2.832	426	4.603	4116	13	0.106	P	1.73	**24.5 ± 4.1**	23.3 ± 8.8	21	12.47 ± 0.64	2.84	52
DFYF3	Eleana Formation (ss)	572112	4102051	1.515	159	14.558	1528	4.605	4116	20	0.612	P	2.00	**27.2 ± 2.4**	21.9 ± 4.0	63	13.09 ± 0.27	2.13	173
DFYF3 (dup)	Eleana Formation (ss)	572112	4102051	0.401	77	3.911	751	4.580	4116	23	0.323	P	1.77	**26.7 ± 3.3**	26.0 ± 6.2	19	10.94 ± 0.70	2.98	46
DFYF4	Eureka Quartzite	579570	4094021	0.600	76	4.253	539	4.607	4116	20	0.758	P	1.90	**36.9 ± 4.6**	47.4 ± 5.3	11	10.50 ± 0.71	2.23	54
DFYF7	Eureka Quartzite	579289	4093685	1.019	191	4.586	860	4.609	4116	20	0.542	P	1.89	**58.0 ± 5.0**	72.6 ± 10.9	38	11.52 ± 0.37	2.24	95

Table 4-1. Apatite Fission-Track Data (continued)

Site	Rock Type	Easting	Northing	ρ_s	Ns	ρi	Ni	ρd	Nd	Grains	Q	χ2	Dpar	Pooled Age	Mean Age	NT	Mean Length	σ	U
RJBD1-1A	Stirling Quartzite	531012	4050377	0.082	137	4.137	707	4.853	4175	22	0.000	F	1.70	53.3 ± 5.2	**67.4 ± 11.9**	73	12.18 ± 0.21	1.79	45
RJBD1-1B	Stirling Quartzite	531012	4050377	1.060	217	4.165	853	4.838	4175	24	0.712	P	1.71	**69.6 ± 5.7**	65.1 ± 11.8	58	11.52 ± 0.26	1.95	49
RJBD1-2	Stirling Quartzite	531012	4050377	0.762	122	3.212	514	4.822	4175	20	0.916	P	1.70	**64.8 ± 6.8**	72.4 ± 18.7	50	11.80 ± 0.25	1.73	37
RJBD1-3	Stirling Quartzite	531012	4050377	0.953	97	4.452	453	4.807	4175	15	0.820	P	1.74	**58.3 ± 6.8**	71.8 ± 13.7	52	11.90 ± 0.30	2.14	48
RJBD1 (all)	Stirling Quartzite	531012	4050377	0.899	573	3.964	2527	4.853	4175	81	0.027	F	1.71	62.3 ± 3.4	**69.1 ± 7.1**	233	11.87 ± 0.13	1.91	45
Previously Published																			
CC-61 (H&S 93)	Pelitic Schist	511207	4061043												**5.6 ± 1.4**				
900008 (H&D 91)	Muscovite Granite	504614	4062871												**6.6**				
IH1-BIO (H&D 93)	pC Basement	551756	3970035												**10.2**				
DKH-IH2 (H&D 93)	pC Basement	550690	3972248												**9.9**				
DKH-JP (H&D 93)	pC Basement	538500	3973665												**8.4**				
988-25 (H&D 93)	Gabbro Diorite	529423	3989528												**6.9**				
89-MP (H&D 93)	pC Basement	522373	3987474												**7.6**				
BM-TH-14ab (H etal 97)	Schist	521999	4082379												**11.1**				

Table 4-1. Apatite Fission Track Data (continued)

Site	Rock Type	Easting	Northing	ρ_s	Ns	ρi	Ni	ρd	Nd	Grains	Q	χ2	Dpar	Pooled Age	Mean Age	NT	Mean Length	σ	U
BF-TH-9AB (H etal 97)	Amphibolite	510361	4082461												**10.0**				
BF-TH-10 (H etal 97)	Schist	510454	4082564												**10.6**				

Notes: Easting and Northing are UTM (Zone 11, NAD 27) locations in meters. All errors are reported at 1σ; zeta calibration factor for analyst RAD of 113.8 ± 2.9 (e.g., Hurford, A.J. and P.F. Green. "The Zeta Calibration of Fission Track Dating." Isotope Geosciences. Vol. 1. pp. 285–317. 1983.) relative to CN-1 dosimeter glass (39 ppm natural uranium) determined using Durango and Fish Canyon Tuff apatite standards irradiated with these samples; mean spontaneous track lengths for Durango and Fish Canyon Tuff apatite standards are 14.47 ± 0.06 µm, and 15.35 ± 0.06 µm, respectively. Rock types are defined in Monsen, et al. (1992). ρs, ρi, and ρd, are spontaneous, induced, and dosimeter fission tracks, respectively, given in units of in 106 tracks per cm2. Ns, Ni, and Nd are the number of spontaneous, induced, and dosimeter fission tracks, respectively. Grains is the number of apatite grains. Q is the probability that χ2 value would be greater than reported for a population of apatite grains having a common history and common kinetic response to that history; χ2 Test, P (pass) for Q 0.05, F (fail) for Q <0.05. Dpar is the mean etch pit diameter parallel to the crystallographic c-axis for the grains measured (Dpar <1.75 typical of near-end-member fluorapatite). Pooled Age is the fission-track age based on sum total of spontaneous and induced tracks for all grains measured (reliable when χ2 Test is P, indicated by bold font) given in Ma. Mean Age is the arithmetic mean of the individual grain ages (reliable when χ2 Test is F, indicated by bold font) given in Ma. NT is the number of track lengths measured. Mean length is average track length in µm. σ is one standard deviation about the mean of the track length measurements. U is the concentration of uranium in ppm.

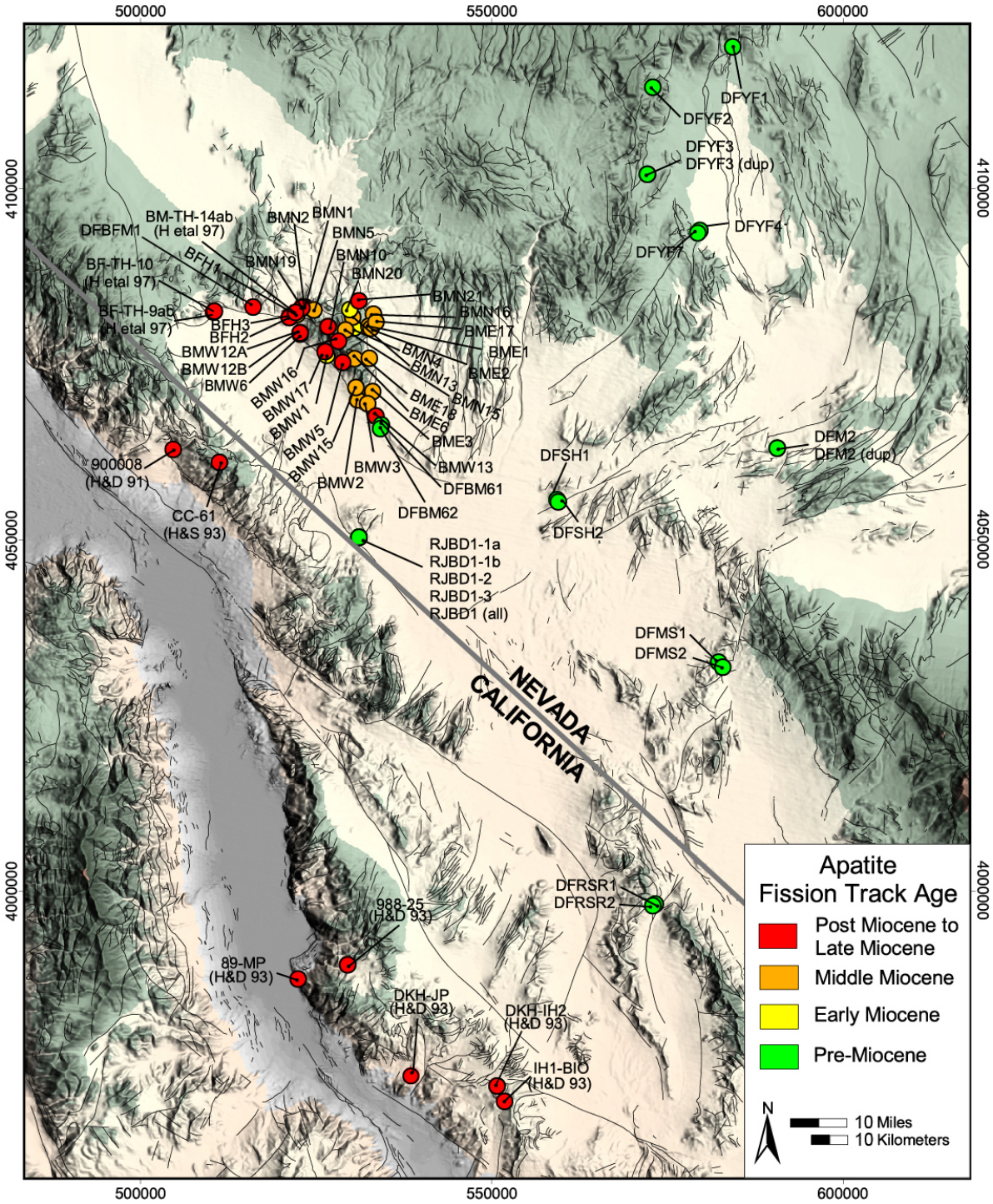

Figure 4-1. Shaded Relief Digital Elevation Model of Southern Nevada and California Showing Locations of Apatite Fission-Track Sample Locations and Ages Sampled for This Study. Other Regional Data Sources Are Indicated Thus: H etal 97 = Hoisch, et al., 1997; H&S 93 = Hoisch and Simpson, 1993; H&D 93 = Holm and Dokka, 1993.

5 ZIRCON FISSION-TRACK THERMOCHRONOLOGY RESULTS

Sixteen fission-track samples were processed for zircon fission-track analysis (Table 5-1). Most of the zircon fission-track ages are much younger than the ages of their host rocks, indicating that the host rocks were heated above the total fission-track annealing temperature of zircon after deposition. With two exceptions, the zircon fission-track ages reflect resetting of the host mineral grains and cooling of the host rocks, presumably during exhumation, through the zircon fission-track closure temperature, rather than being inherited from a previously eroded terrain or recording primary cooling.

One exception is the sample from the silicic porphyry dike (BME-2; Table 5-1) sampled from Bare Mountain, which yields a zircon fission-track age of 11.9 ± 1.2 Ma, concordant with the apatite fission-track age of 12.3 ± 3.2 Ma. A conventional K/Ar age of 13.8 ± 0.2 Ma was measured from biotite from this dike (Monsen, et al., 1992). Based on data from Marvin, et al. (1989), Noble, et al. (1991), Monsen, et al. (1992), and Weiss (1996), conventional K/Ar and Ar-40/Ar-39 dates from the silicic porphyry dikes along eastern Bare Mountain, of which this is part, range from 14.9 to 13.8 Ma. However, textural features and K/Ar dates from alunite indicate epithermal and hydrothermal activity contemporaneous with the later stages of silicic volcanism (circa 11.0 to 12.5 Ma), especially associated with altered margins of the silicic porphyry dikes. Our apatite and zircon fission-track ages are consistent with resetting due to epithermal or hydrothermal activity, or the fission-track ages can be considered concordant with the conventional K/Ar biotite age.

The second exception is Eureka quartzite (DFM-2) sampled from the south side of Frenchman Flat at Mercury Ridge, which yielded a fission-track age older than the depositional age of the rock. This age relationship suggests that the fission-track age records provenance age of the host rock from which the Eureka quartzite grains were derived. The Eureka quartzite at this location was apparently never buried sufficiently deep to reset the zircon fission tracks. Apatite grains from the same sample yield Cretaceous ages, indicating that the apatite grains were reset after deposition in the Ordovician.

In addition to our 16 new zircon fission-track ages, we include 15 published ages from the Black Mountains (Holm and Dokka, 1993), Funeral Mountains (Holm and Dokka, 1991), and Bullfrog Hills, and northwest corner of Bare Mountain (Hoisch, et al., 1997). Like the apatite fission-track ages, zircon fission-track ages fall into a population of pre-Miocene ages and a population of Miocene and younger ages (Figures 5-1 and 5-2). Pre-Miocene ages generally lie to the east of Miocene ages at the latitude of the Funeral Mountains, Bullfrog Hills, and Bare Mountain (Figure 5-1; see Figure 1-1 for place names). Zircon ages range from 25 to 115 Ma (Figures 5-1 and 5-2). As with the apatite fission-track ages, we subdivided the Miocene and younger zircon fission-track ages into three groups: (i) Early Miocene (16.6 to 23.7 Ma), (ii) Middle Miocene (11.2 to 16.6 Ma), and (iii) Late Miocene (5.3 to 11.2 Ma) and younger (Figures 5-1 and 5-2). The youngest ages are found along the eastern margin of Death Valley in the Funeral Mountains and Black Mountains. Miocene cooling ages are generally younger to the west or northwest. The Funeral Mountains and Bare Mountain include ages belonging to both the Miocene and pre-Miocene populations.

Table 5-1. Zircon Fission-Track Data

Site	Rock Type	Easting	Northing	ρ_s	N_s	ρ_i	N_i	ρ_d	N_d	Grains	Q	χ^2	Age	U	Analyst
BFH-1	Wood Canyon Formation (schist)	522200	4082050	2.09	155	4.450	330	0.20	1272	11	0.89	P	15.7 ± 1.5	231	AEB
BFH-2	Wood Canyon Formation (schist)	521130	4081680	2.80	246	7.460	664	0.20	1272	11	0.01	F	13.7 ± 1.0	385	AEB
BMW-6	Stirling Quartzite (D member)	522690	4079300	2.58	554	5.370	1155	0.19	1223	20	0.16	P	15.3 ± 0.8	278	AEB
BME-2	Quartz latite dike	532780	4080120	2.45	135	6.840	376	0.20	1260	8	0.56	P	11.9 ± 1.2	327	AEB
BMN-5	Zabriskie Quartzite	524640	4082730	2.73	579	3.580	759	0.19	1248	16	0.99	P	24.9 ± 1.4	184	AEB
BMN-10	Zabriskie Quartzite	526671	4080373	4.49	628	4.200	588	0.19	1235	20	0.56	P	34.5 ± 2.0	215	AEB
BMW-2	Wood Canyon Formation (quartzite; lower member, unit A)	530880	4069920	6.31	606	4.840	465	0.19	1223	13	0.37	P	41.5 ± 2.6	266	AEB
BMW-3	Stirling Quartzite (D member)	532300	4069380	5.10	1291	3.600	911	0.19	1217	17	0.24	P	45.1 ± 2.0	187	AEB
BME-3	Wood Canyon Formation (quartzite)	533000	4071100	3.61	419	2.970	344	0.20	1260	16	0.60	P	40.2 ± 2.9	153	AEB
BMN-4	Zabriskie Quartzite	530360	4080190	18.36	1964	2.040	216	0.19	1248	20	0.34	P	297.0 ± 21.3	107	AEB
BMN-15	Zabriskie Quartzite	529163	4079903	16.50	2230	1.940	221	0.19	1235	20	0.28	P	275.1 ± 19.5	100	AEB
DFSH-1	Zabriskie Quartzite	559253	4055732	11.62	729	0.925	58	0.56	2053	10	0.75	P	458 ± 65	108	RAD
DFSH-2	Wood Canyon Formation (quartzite)	559409	4055393	10.60	631	1.140	68	0.57	2053	10	0.11	P	349 ± 46	127	RAD
DFBM61	Zabriskie Quartzite	534210	4066361	8.48	662	0.794	62	0.59	2053	10	0.13	P	409 ± 56	104	RAD
DFBM62	Zabriskie Quartzite	534135	4065850	10.02	782	0.961	75	0.60	2053	10	0.01	F	463 ± 75	129	RAD
DFM2	Eureka Quartzite	590572	4063062	18.01	784	1.330	58	0.61	2053	9	0.00	F	688 ± 134	139	RAD
900009 (H&D 91)	Muscovite Granite	504614	4062871										10.6		
IH1-BIO (H&D 93)	pC Basement	551756	3970035										>89.9		
DKH-IH2 (H&D 93)	pC Basement	550690	3972248										15.0		
DKH-JP (H&D 93)	pC Basement	538500	3973665										11.4		
AM2a-M (H&D 93)	pC Basement	529759	3979177										18.7		
DKH-FS (H&D 93)	Gabbro Diorite	529979	4002655										6.3		
DKH-SMG (H&D 93)	Granite	531557	3980662										8.8		
89-CC (H&D 93)	pC Basement	523851	3995981										7.8		
DKH-IH2 (H&D 93)	pC Basement	550690	3972248										15.0		
DKH-JP (H&D 93)	pC Basement	538500	3973665										11.4		
AM2a-M (H&D 93)	pC Basement	529759	3979177										18.7		
DKH-FS (H&D 93)	Gabbro Diorite	529979	4002655										6.3		
DKH-SMG (H&D 93)	Granite	531557	3980662										8.8		
89-CC (H&D 93)	pC Basement	523851	3995981										7.8		
988-25 (H&D 93)	Gabbro Diorite	529423	3989528										7.5		
89-MP (H&D 93)	pC Basement	522373	3987474										7.9		
BWT-B (H&D 93)	pC Basement	521275	4126312										8.7		
TQM-GW-B (H&D 93)	Granite	557384	3983751										7.5		
BM-TH-14ab (H etal 97)	Schist	521999	4082379										12.6		
BF-TH-9ab (H etal 97)	Amphibolite	510361	4082461										9.2		
BF-TH-10 (H etal 97)	Schist	510454	4082564										11.2		

Notes: Explanations of table headings are the same as in Table 1. Ages determined using zeta calibration factor of 335 ± 20 relative to SRM 962a dosimeter glass (analyst AEB) or 135.0 ± 3.8 relative to CN-1 dosimeter glass (analyst RAD). The age for sample BFH-2, which failed the χ^2 test, is the mean age instead of the pooled age.

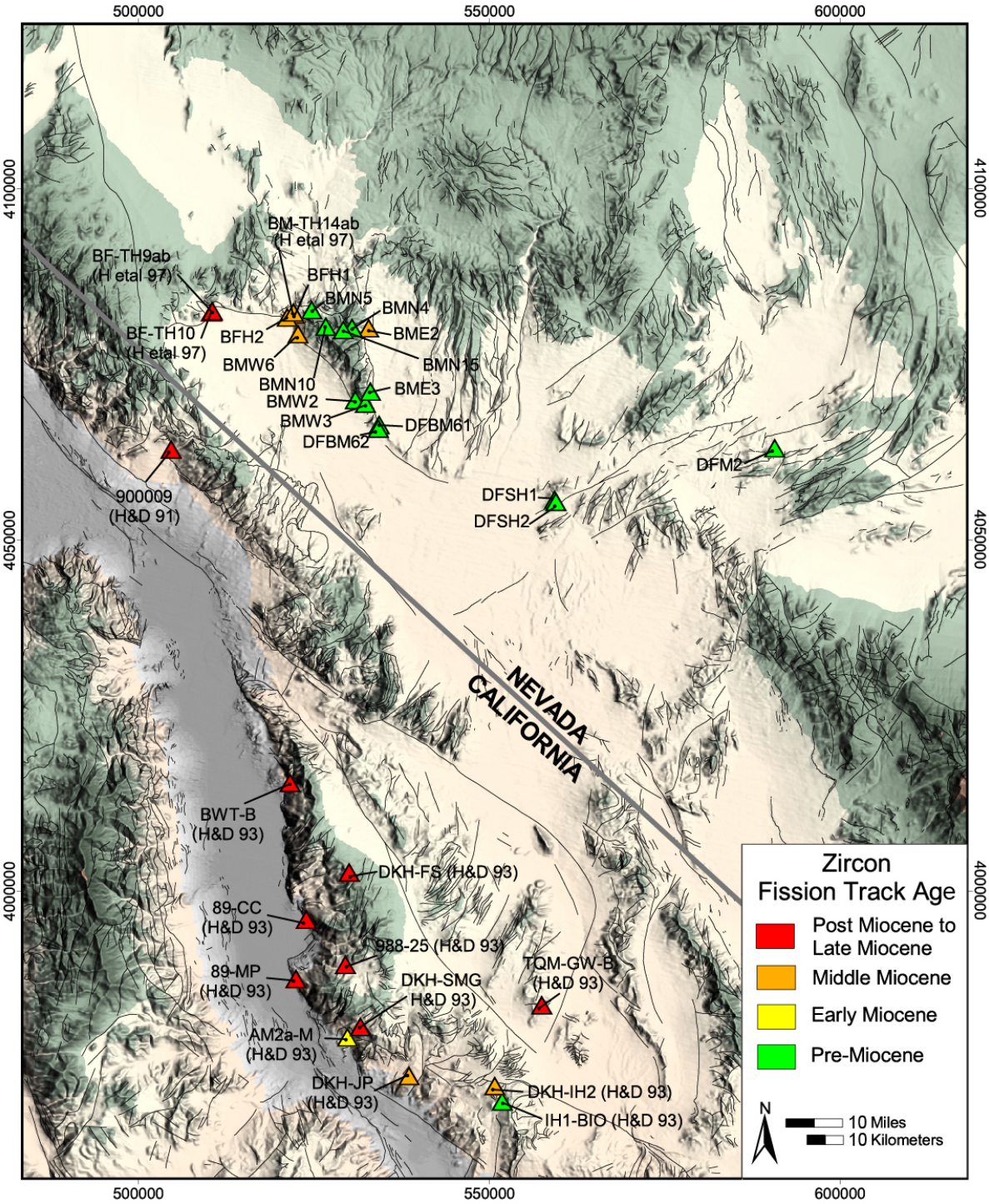

Figure 5-1. Shaded Relief Digital Elevation Model of Southern Nevada and California Showing Locations of Zircon Fission-Track Sample Locations and Ages Sampled for This Study. Other Regional Data Sources Are Indicated Thus: H et al 97 = Hoisch, et al., 1997; H&S 93 = Hoisch and Simpson, 1993; H&D 93 = Holm and Dokka, 1993.

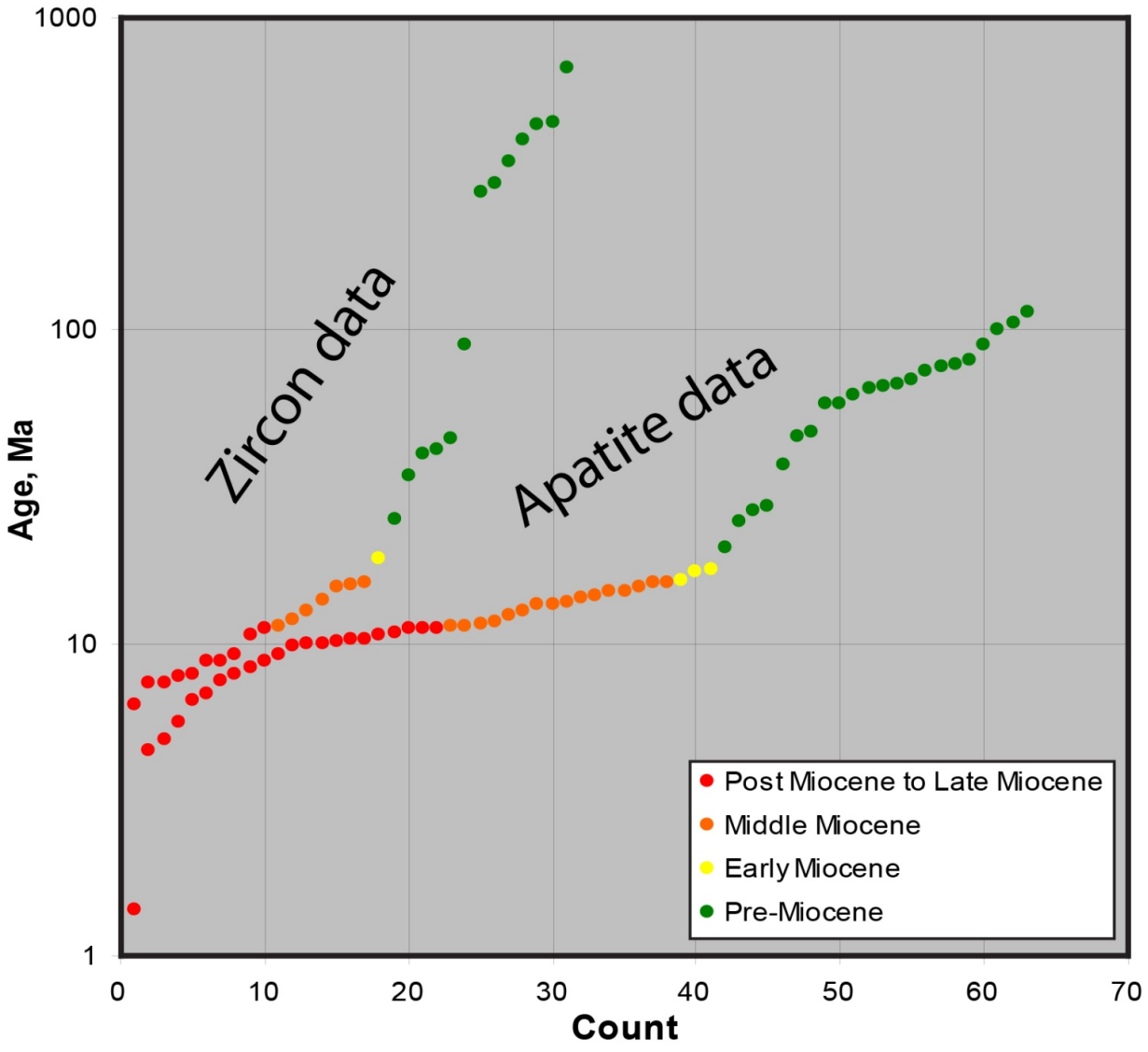

Figure 5-2. Age Versus Count (Cumulative Number of Data Points) Plots of Zircon and Apatite Cooling Ages Based on Data in Tables 4-1 and 5-1. Ages for Both Apatite and Zircon Data Are Color Coded as in Figures 4-1 and 5-1.

6 DISCUSSION

Large normal fault displacements can thin the crust and exhume rocks from depths beneath the apatite- and zircon-annealing depths. This is especially true where the absence of syndeformational sedimentation permits the footwall of the system to respond to unloading by isostatic uplift (Stewart, 1983; Wernicke, et al., 1987; Wernicke and Axen, 1988; Wernicke, 1992; Asmerom, et al., 1990; Block and Royden, 1990). Prior to deformation, apatite and zircon grains within the footwall of the extensional system are hotter than their respective closure temperatures and are continuously annealed [Figure 6-1(A)].

Uplift generated by displacement of the hanging wall causes the footwall and its associated population of apatites and zircons to move toward the Earth's surface and down the geothermal gradient to progressively cooler conditions. The fission-track ages represent the time elapsed since the mineral passed through its closure temperature on its way to the Earth's surface. Because the unroofing process is progressive and at large scale directional, the pattern of cooling ages in the exposed footwall will show a pattern of decreasing ages in the direction of hanging wall displacement [Figure 6-1(B)]. Fault slivers stranded on the footwall will contain fission-track younging patterns broadly similar to the fundamental footwall [Figure 6-1(C)]. Structural complexities in some areas, such as the stranding of a hanging wall fault sliver, may partially occlude this broad pattern [Figure 6-1(C)]. Based on this model, Bare Mountain, the Bullfrog Hills, the Funeral Mountains, and the Black Mountains were all unroofed differentially during the Miocene (Maldonado, 1990; Holm and Dokka, 1991; Hoisch and Simpson, 1993; Serpa and Pavlis, 1996), and this interpretation is in accord with large-scale structural relationships and small-scale deformation features, including brittle extensional structures that overprint ductile extensional deformation fabrics (Wernicke and Axen, 1988; Wernicke, 1995, 1992).

In this work (Figures 4-1 and 5-1), we note that the eastern half of Bare Mountain exhibits pre-Miocene cooling through 250 °C [482 °F], followed by Miocene cooling through 130–146 °C [266–295 °F]. Northwest Bare Mountain cooled through both 250 °C [482 °F] and 130–146 °C [266–295 °F] since the beginning of the Miocene. South and east of Bare Mountain, including the southeasternmost Funeral Mountains and the Resting Spring Range but excluding the Black Mountains, apatite closure ages are pre-Miocene. West of this broadly defined line, apatite ages show a consistent younging trend to the west.

We interpret Miocene and younger apatite and zircon cooling ages to indicate exhumation of the rocks through the 130–146 °C [266–295 °F] (apatite) and 250 °C [482 °F] (zircon) closure temperatures in response to the west-northwest-directed tectonic removal of overlying crust. The initiation of the breakaway at Bare Mountain occurred at about 13 Ma (this work and Hoisch, et al., 1997). Our fission-track results do not indicate tectonic exhumation east of Bare Mountain, which refutes earlier interpretations by Hamilton (1988, 1987) and Scott (1990) that a shallow regional detachment extends beneath and east of Yucca Mountain. We suggest that the Death Valley–Furnace Creek fault zone (Figure 3-1) represents the current position of the easternmost surface trace of the west-northwestward-moving hanging wall (consistent with Stewart, 1983, and Serpa and Pavlis, 1996). Projecting the apatite age data horizontally and parallel to the traces of the extensional fault segments onto transects that are parallel to the regional extension direction over the last 12 million years (represented by the Furnace Creek fault trace; McQuarrie and Wernicke, 2005) yields graphs which illustrate the sharp break between older (pre-Miocene) ages to the east-southeast and younger (Miocene) ages to the west-northwest [Figures 6-2(B,C)]. Considering only the Miocene and younger ages

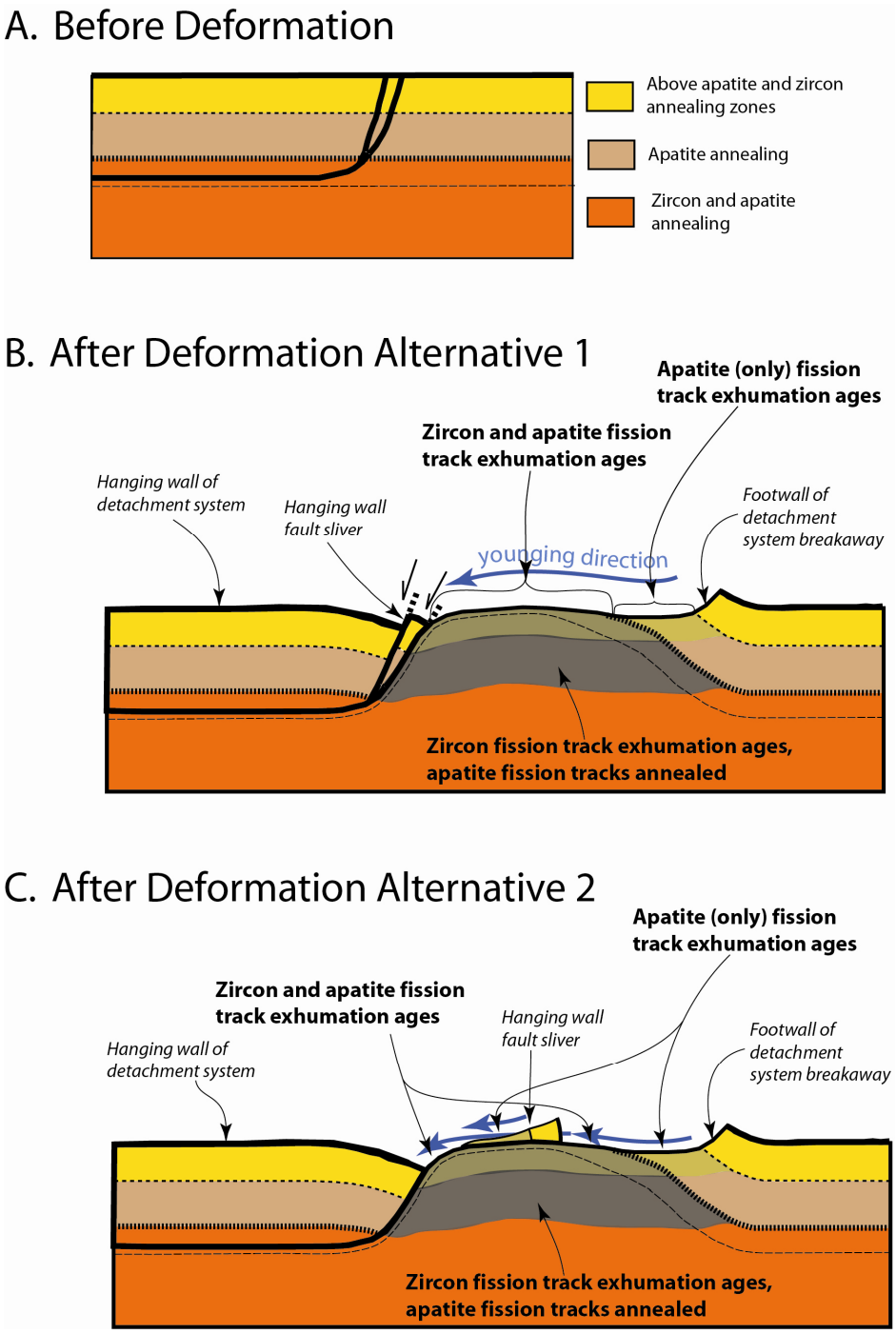

Figure 6-1. Models of Faulting, Exhumation, and Isostatic Adjustment Illustrating Unroofing of Rocks With Reset Apatite and Zircon Ages: (A) Crustal Cross Section Before Deformation. Dashed Line Within Orange Is an Arbitrary Marker for Reference. (B) Detachment Faulting With Isostatic Adjustment of the Footwall and Illustrating the Case Where a Single Hanging Wall Fault Sliver Is Adjacent to the Main Hanging Wall Block. (C) Detachment Faulting With Isostatic Adjustment of the Footwall and Illustrating the Case Where a Single Hanging Wall Fault Sliver Is Stranded on the Footwall Block.

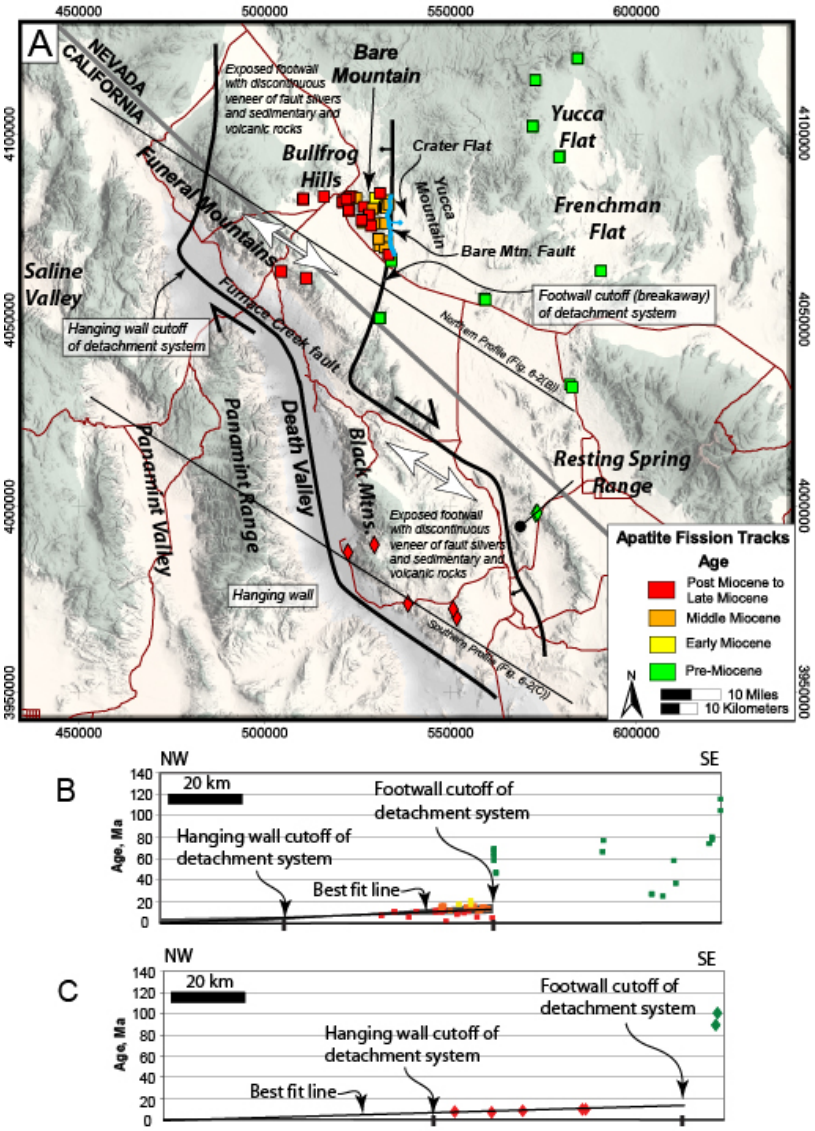

Figure 6-2. (A) Digital Shaded Relief Map Illustrating the Interpreted Position of the Breakaway Fault, Interpretation of Domains With Respect to Detachment System, and Location of Transects in (B) and (C). Squares are Horizontally Projected Onto the Northern Transect Line [Figure 6-2(B)] Along an Azimuth of 190°, Diamonds Are Horizontally Projected Onto the Southern Transect Line [Figure 6-2(C)] Along an Azimuth of 170°. (B) Transect Along Azimuth 123°, Parallel to the Furnace Creek Fault Zone Sharing Apatite Fission-Track Cooling Ages Plotted Against Distance Along Transect. Color Coding as in (A). Gray Area Represents Range of Best Fit Lines Within ±1 Standard Deviation From the Mean. Least Squares Best Fit Line to the Miocene and Younger Data Is Provided. The Southeastern Projection to 13 Ma Coincides With the Inferred Trace of the Footwall Cutoff of the Detachment System. The Northwestward Projection to 0 Ma Indicates That Rocks at the Far Northwest End of the Transect, at the Appropriate Depth, Are Currently Passing Through the Apatite Closure Geotherm. The Inverse Slope of the Best Fit Line Is 10 mm Per Year [0.394 in/yr]. (C) Transect Along Azimuth 123° (Parallel to the Furnace Creek Fault Zone), Apatite Fission-Track Cooling Ages Are Plotted Against Distance Along Transect. The Inverse Slope of the Best Fit Line Is 11 mm Per Year [0.433 in/yr].

[Figures 6-2(B,C)] reveals a west-northwest younging trend that results from migration of the apatite cooling front. Migration of the front was comparable in the Bare Mountain–Bullfrog Hills area {10 mm/yr [0.394 in/yr]; Figure 6-2(B)} and in the Black Mountains {11 mm/yr [0.433 in/yr]; Figure 6-2(C)}. Projecting the Black Mountain data eastward to 13 Ma indicates that the location of the breakaway in that area was just to the west of the Resting Spring Range [Figure 6-2(A)]. This also agrees with Stewart's (1983) placement of the Panamint Mountains prior to faulting and subsequent restored positions of the Panamint Range interpreted by Snow (1994), Serpa and Pavlis (1996), and Snow and Wernicke (2000).

South of Bare Mountain, the position of the breakaway is constrained between the location for our sample locality RJBD1 along the northeastern margin of the Funeral Mountains (mean apatite age of 69.1 Ma), and samples CC-61 (apatite age of 5.6 Ma; Hoisch and Simpson, 1993) and 900008 (apatite age of 6.6 Ma; Holm and Dokka, 1991). From here the trace must step laterally to pass to the east of the Late Miocene ages from the Black Mountains and west of the 89.3 Ma apatite fission-track age from the Resting Spring Range. This step corresponds to the surface trace of the Furnace Creek fault. The precise location of the footwall cutoff in the vicinity of the Funeral Mountains is not well constrained by our data. However, although Workman, et al. (2002) show the location from which we collected sample RJBD1 as being separated from the main Funeral Mountains by a fault, more detailed mapping by Wright and Troxel (1993) shows that the geologic layers and layer orientations (including marker beds and folds) at RJBD1 correlate with geology along strike in the Funeral Mountains. We have, therefore, chosen to link the trace directly to the Furnace Creek fault zone as shown in Figure 6-2(A), but there may be more complexity than this indicates.

Large-magnitude displacement on a dipping fault (e.g., in the vicinity of the detachment-fault breakaway) results in differential unloading and, therefore, differential footwall uplift. This differential uplift tilts the footwall in the direction opposite to the hanging wall transport direction (Figure 6-1). This differential uplift is controlled by lateral variation in thickness of removed hanging wall rock above the dipping fault. Apatite and zircon grains deeper than their corresponding annealing depths are progressively unroofed and cooled, resulting in accumulation of fission tracks and younging of fission-track ages in the direction of hanging wall transport. Rocks exposed in the exhumed footwall will contain mineral grains that exhibit a variety of cooling age patterns depending upon the depth to detachment of the major fault system, the geothermal gradient during exhumation, and the depth of erosion following footwall uplift. Our interpretation of detachment faulting related to crustal exhumation in the Death Valley region is illustrated in Figure 6-1. Exhumed footwall rocks adjacent to the surface trace of the breakaway fault and initially shallower in the crust than the apatite fission-track closure temperature geotherm exhibit preexhumation ages for both apatites and zircons. Within the footwall and in the direction of transport of the hanging wall, there will be a zone in which apatite will yield exhumation cooling ages but zircon will not. Finally, there is a zone in which both zircon and apatite yield exhumation cooling ages. Fission-track ages for a given mineral will be younger in the direction of transport of the hanging wall reflecting progressive exhumation (e.g., Holm and Dokka, 1993, 1991; Hoisch and Simpson, 1993; Hoisch, et al., 1997). Complications to this general pattern arise if slivers of the hanging wall are left on the exhumed footwall [e.g., Figure 6-1(C); Wernicke and Axen, 1988; Wernicke, 1992]–each sliver, however, represents a small version of the overall footwall pattern.

Our interpreted configuration of the footwall and hanging wall cutoffs of the Death Valley–Furnace Creek regional detachment system places Crater Flat basin immediately adjacent to the footwall cutoff and in the footwall of the system [Figure 6-2(A)]. Yucca Mountain lies at the eastern edge of Crater Flat basin and is a series of cuestas formed by west-dipping normal

faults with displacements on the order of a few hundreds of meters [up to more than 1,000 ft] (e.g., Ferrill, et al., 1999; Ferrill and Morris, 2001; Morris, et al., 2004). Crater Flat basin is a half-graben controlled by displacement on the east-dipping Bare Mountain fault, which has a maximum displacement of 3 to 5 km [1.9 to 3.1 mi] (Faulds, et al., 1994; Ferrill, et al., 1996b; Brocher, et al., 1998). Faulting at Yucca Mountain and on the Bare Mountain fault was at least in part contemporaneous with Miocene tuff emplacement (Carr, 1990; Monsen, et al., 1992), began approximately 13 million years ago, and has continued into the Quaternary (Ferrill, et al., 1997, 1996b). Fault displacements and associated extensions within the Bare Mountain–Crater Flat–Yucca Mountain system are one to two orders of magnitude less than those faults in the Bullfrog Hills (just north and west of Bare Mountain) and within the Death Valley–Furnace Creek detachment system. Fault slivers within the Bullfrog Hills contain a highly extended sequence of Miocene volcanic rocks (Maldonado, 1990). The Bare Mountain–Crater Flat–Yucca Mountain system likely represents footwall damage that developed coevally with the large Miocene displacement on the Death Valley–Furnace Creek detachment system and its consequent footwall uplift (Stamatakos, et al., 2011).

7 CONCLUSIONS

Apatite and zircon fission-track cooling ages from the Death Valley region of southern Nevada show (i) a belt of Miocene ages and a broad region of pre-Miocene ages; (ii) the belt of Miocene ages corresponds to an area of large-magnitude crustal extension by normal faulting and is segmented, with an area of Miocene fission-track ages in the Bare Mountain–Funeral Mountains area and in the Black Mountains; (iii) the eastern edge of Miocene fission-track ages is mapped in Bare Mountain and the Funeral Mountains, then steps eastward (to the south) to east of the Black Mountains and west of the Resting Spring Range; and (iv) fission-track ages within the belt of Miocene exhumation young westward, suggesting progressive westward or northwestward progression of exhumation.

We interpret that early Miocene apatite ages are near the breakaway (footwall cutoff) of the regional detachment faulting and that the original crustal faults which defined the edge of the detachment system may have originally been separate normal faults linked by a transfer zone, similar to fault system architecture in the Panamint Valley–Saline Valley region today. Migration rates of the cooling front in the footwall of this system are on the order of 10 to 11 mm/yr [0.394 to 0.433 in/yr]. Extrapolation of apatite fission-track closure ages from two transects across the eastern margin of the Death Valley region suggests that exhumation along the eastern margin of the system continues beneath Death Valley today. East of the footwall cutoff of this system, extensional basins, such as the Crater Flat basin, either did not experience enough extension in the last 13 million years to produce footwall exhumation sufficient to be recorded in cooling ages, or Miocene basin filling with volcanic and alluvial material occurred too rapidly for isostatic footwall uplift to occur.

8 REFERENCES

Asmerom, Y., J.K. Snow, D.K. Holm, S.B. Jacobsen, B.P. Wernicke, and D.R. Lux. "Rapid Uplift and Crustal Growth in Extensional Environments: An Isotopic Study From the Death Valley Region, California." *Geology*. Vol. 18. pp. 223–226. 1990.

Atwater, T. "Implications of Plate Tectonics for the Cenozoic Tectonic Evolution of Western North America." Geological Society of American Bulletin. Vol. 81. pp. 3,513–3,536. 1970.

Axen, G.J., W.J. Taylor, and J.M. Bartley. "Space-Time Patterns and Tectonic Controls of Tertiary Extension and Magmatism in the Great Basin of the Western United States." *Geological Society of America Bulletin*. Vol. 105. pp. 56–76. 1993.

Block, L. and L.H. Royden. "Core Complex Geometries and Regional Scale Flow in the Lower Crust." *Tectonics*. Vol. 9. pp. 557–567. 1990.

Brandon, M.T. and J.A. Vance. "Tectonic Evolution of the Cenozoic Olympic Subduction Complex, Washington State, as Deduced From Fission Track Ages for Detrital Zircons." *American Journal of Science*. Vol. 292. pp. 565–636. 1992.

Brocher, T.M., W.C. Hunter, and V.E. Langenheim. "Implications of Seismic Reflection and Potential Field Geophysical Data on the Structural Framework of the Yucca Mountain-Crater Flat Region, Nevada." *Geological Society of America Bulletin*. Vol. 110. pp. 947–971. 1998.

Brun, J.-P., D. Sokoutis, and J. Van Den Driessche. "Analogue Modeling of Detachment Fault Systems and Core Complexes." *Geology*. Vol. 22. pp. 319–322. 1994.

Burchfiel, B.C., K.V. Hodges, and L.H. Royden. "Geology of Panamint Valley-Saline Valley Pull-Apart System, California, Palinspastic Evidence for Low-Angle Geometry of a Neogene Range-Bounding Fault." *Journal of Geophysical Research*. Vol. 93. pp. 10,422–10,426. 1987.

Carlson, W.D., R.A. Donelick, and R.A. Ketcham. "Variability of Apatite Fission-Track Annealing Kinetics: I. Experimental Results." *American Mineralogist*. Vol. 84. pp. 1,213–1,223. 1999.

Carr, W.J. "Styles of Extension in the Nevada Test Site Region, Southern Walker Lane Belt; An Integration of Volcano-Tectonic and Detachment Fault Models, in Basin and Range Extensional Tectonics Near the Latitude of Las Vegas, Nevada." B.P. Wernicke, ed. Geological Society of America Memoir 176. pp. 283–303. Boulder, Colorado: Geological Society of America. 1990.

Cowan, D.S., T.T. Cladouhos, and J.K. Morgan. "Structural Geology and Kinematic History of Rocks Formed Along Low-Angle Normal Faults, Death Valley, California." GSA Bulletin. Vol. 115. pp. 1,230–1,248. 2003.

Dixon, T.H., M. Miller, F. Farina, H. Wang, and D. Johnson. "Present-Day Motion on the Sierra Nevada Block and Some Tectonic Implications for the Basin and Range Province, North American Cordillera." *Tectonics*. Vol. 19. pp. 1–24. 2000.

Dixon, T.H., S. Robaudo, J. Lee, and M.C. Reheis. "Constraints on Present-day Basin and Range Deformation From Space Geodesy." *Tectonics*. Vol. 14. pp. 755–772. 1995.

Dodson, M.E. "Theory of Cooling Ages." *Lectures in Isotope Geology*. E. Jaeger, J.C. Hunziker, eds. Berlin, Germany: Springer Verlag. p. 329. 1979.

_____. "Closure Temperature in Cooling Geochronological and Petrological Systems." *Contributions to Mineralogy and Petrology.* Vol. 40. pp. 259–274. 1973.

Donelick, R.A., P.B. O'Sullivan, and R.A. Ketcham. "Apatite Fission-Track Analysis." *Mineralogy and Geochemistry*. Vol. 58. pp. 49–94. 2005.

Dumitru, T.A. "Fission-Track Geochronology in Quaternary Geochronology; Applications in Quaternary Geology and Paleoseismology, Volume 1." J.S. Noller, J.M. Sowers, and W.R. Lettis, eds. Washington, DC: American Geophysical Union, Geophysical Monograph Series. 1999.

Faulds, J.E., J.W. Bell, D.L. Feuerbach, and A.R. Ramelli. "Geologic Map of the Crater Flat Area, Nye County, Nevada." Nevada Bureau of Mines and Geology Map 101. Scale 1:24,000. 1994.

Ferrill, D.A. and A.P. Morris. "Displacement Gradient and Deformation in Normal Fault Systems." *Journal of Structural Geology*. Vol. 23. pp. 619–638. 2001.

Ferrill, D.A., J.A. Stamatakos, and D. Sims. "Normal Fault Corrugation: Implications for Growth and Seismicity of Active Normal Faults." *Journal of Structural Geology.* Vol. 21. pp. 1,027–1,038. 1999.

Ferrill, D.A., J.A. Stamatakos, and H.L. McKague. "Quaternary Slip History of the Bare Mountain Fault (Nevada) From the Morphology and Distribution of Alluvial Fan Deposits." *Geology*. Vol. 25. p. 190. 1997.

Ferrill, D.A., G.L. Stirewalt, D.B. Henderson, J.A. Stamatakos, K.H. Spivey, and B.P. Wernicke. NUREG/CR–6401, "Faulting in the Yucca Mountain Region, Critical Review and Analyses of Tectonic Data from the Central Basin and Range." Washington, DC: U.S. Nuclear Regulatory Commission. 1996a.

Ferrill, D.A., J.A. Stamatakos, S.M. Jones, R. Rahe, H.L. McKague, R.H. Martin, and A.P. Morris. "Quaternary Slip History of the Bare Mountain Fault (Nevada) From the Morphology and Distribution of Alluvial Fan Deposits." *Geology*. Vol. 24. pp. 559–562. 1996b.

Ferrill, D.A., G.L. Stirewalt, D.B. Henderson, J.A. Stamatakos, A.P. Morris, B.P. Wernicke, and K.H. Spivey. "Faulting in the Yucca Mountain Region: Critical Review and Analyses of Tectonic Data From the Central Basin and Range." CNWRA 95-017. San Antonio, Texas: Center for Nuclear Waste Regulatory Analyses. 1995.

Foster, D.A., A.J. Gleadow, S.J. Reynolds, and P.G. Fitzgerald. "Denudation of Metamorphic Core Complexes and the Reconstruction of the Transition Zone, West Central Arizona: Constraints From Apatite Fission Track Thermochronology." *Journal of Geophysical Research*. Vol. 98, B2. pp. 2,167–2,185. 1993.

Frisch, W., M. Meschede, and R. Blakey. "Plate Tectonics: Continental Drift and Mountain Building." Berlin, Germany: Springer Verlag. 212 pp. 2011.

Gleadow, A.J.W. "Fission Track Dating Methods: What Are the Real Alternatives?" *Nuclear Tracks*. Vol. 5. pp. 3–14. 1981.

Harland, W.B. "Tectonic Transpression in Caledonian Spitsbergen." *Geological Magazine*. Vol. 108. pp. 27–41. 1971.

Hamilton, W.B. "Detachment Faulting in the Death Valley Region, California and Nevada." M.D. Carr and J.C. Yount, eds. *Geologic and Hydrologic Investigations of a Potential Nuclear Waste Disposal Site at Yucca Mountain, Southern Nevada*. United States Geological Survey Bulletin 1790. pp. 51–85. 1988.

_____ "Crustal Extension in the Basin and Range Province, Southwestern United States, Continental Extensional Tectonics." M.P. Coward, J.F. Dewey, and P.L. Hancock, eds. London, England: Geological Society Special Publications 28. pp. 155–176. 1987.

Harrison, T.M. and I. MacDougall. "Investigations of an Intrusive Contact, Northwest Nelson, New Zealand-1. Thermal, Chronological and Isotropic Constraints." *Geochimica et Cosmochimica Acta*. Vol. 44. pp. 1,985–2,003. 1980.

Hayman, N.W. "Shallow Crustal Fault Rocks From the Black Mountain Detachments, Death Valley, California." *Journal of Structural Geology*. Vol. 28. pp. 1,767–1,784. 2006.

Hodges, K.V., L.W. McKenna, J. Stock, J. Knapp, L. Page, K. Sternlof, D. Silverberg, G. Wüst, and J.D. Walker. "Evolution of Extensional Basins and Basin and Range Topography West of Death Valley, California." *Tectonics*. Vol. 8. pp. 453–467. 1989.

Hodges, K.V., J.D. Walker, and B.P. Wernicke. "Footwall Structural Evolution of the Tucki Mountain Detachment System, Death Valley Region, Southeastern California." M.P. Coward, J.F. Dewey, and P.L. Hancock, eds. *Continental Extensional Tectonics*. Geological Society Special Publication No. 28. pp. 393–408. 1987.

Hoisch, T.D., M.T. Heizler, and R.E. Zartman. "Timing of Detachment Faulting in the Bullfrog Hills and Bare Mountain Area, Southwestern Nevada: Inferences from 40Ar/39Ar, K-Ar, U-Pb, and Fission Track Thermochronology." *Journal of Geophysical Research*. Vol. 102. pp. 2,815–2,833. 1997.

Hoisch, T.D. and C. Simpson. "Rise and Tilt of Metamorphic Rocks in the Lower Plate of a Detachment in the Funeral Mountains, Death Valley, California." *Journal of Geophysical Research*. Vol. 98. pp. 6,805–6827. 1993.

Holm, D.K. and R.K. Dokka. "Interpretation and Tectonic Implications of Cooling Histories: An Example From the Black Mountains, Death Valley Extended Terrane, California." *Earth and Planetary Science Letters*. Vol. 116. pp. 63–80. 1993.

_____. "Major Late Miocene Cooling of the Middle Crust Associated with Extensional Orogenesis in the Funeral Mountains, California." *Geophysical Research Letters*. Vol. 18. pp. 1,775–1,778. 1991.

Ketcham, R.A., R.A. Donelick, and W.D. Carlson. "Variability of Apatite Fission-Track Annealing Kinetics: III. Extrapolation to Geological Time Scales." *American Mineralogist*. Vol. 84. pp. 1,235–1,255. 1999.

McKague, H.L., D. Ferrill, K. Smart, J. Stamatakos, D. Waiting. "Synthesis Report for Yucca Mountain Region Tectonic Models." San Antonio, Texas: Center for Nuclear Waste Regulatory Analyses. 2010.

McQuarrie, N. and B.P. Wernicke. "An Animated Tectonic Reconstruction of Southwestern North America Since 36 Ma." *Geosphere*. Vol. 1. pp. 147–172. 2005.

Maldonado, F. "Structural Geology of the Upper Plate of the Bullfrog Hills Detachment Fault System, Southern Nevada." *Geological Society of America Bulletin*. Vol. 102. pp. 992–1,006. 1990.

Marvin, R.F., H.H. Mehnert, and C.W. Naeser. "U.S. Geological Survey Radiometric Ages Compilation 'C', Part 3. California and Nevada." Isochron/West. No. 52. pp. 3–11. 1989.

Miller, M.B. and T.L. Pavlis. "The Black Mountains Turtlebacks: Rosetta Stones of Death Valley tectonics." *Earth-Science Reviews*. Vol. 73. pp. 115–138. 2005.

MIT 1985 Field Geophysics Course and S. Biehler. "A Geophysical Investigation of the Northern Panamint Valley, Inyo County, California: Evidence for Possible Low-Angle Normal Faulting at Shallow Depth in the Crust." *Journal of Geophysical Research*. Vol. 92, No. B10. pp. 10,427–10,441. 1987.

Monsen, S.A., M.D. Carr, M.C. Reheis, and P.A. Orkild. "Geologic Map of Bare Mountain, Nye County, Nevada." U.S. Geological Survey Miscellaneous Investigations Series, Map I-2201. Scale 1:24 000. 1992.

Morris, A.P., D.A. Ferrill, D.W. Sims, N. Franklin, and D.J. Waiting. "Patterns of Fault Displacement and Strain at Yucca Mountain, Nevada." *Journal of Structural Geology*. Vol. 26. pp. 1,707–1,725. 2004.

Naeser, C.W. and F. Maldonado. "Fission-Track Dating of the Climax and Gold Meadows Stocks, Nye County, Nevada, in Shorter Contributions to Isotope Research in the Western United States." U.S. Geological Survey Professional Paper 1199-E. pp. E45–E47. 1981.

Noble, D.C., S.I. Weiss, and E.H. McKee. "Magmatic and Hydrothermal Activity, Caldera Geology, and Regional Extension in the Western Part of the Southwestern Nevada Volcanic Field." *Geology and Ore Deposits of the Great Basin*. G.L. Raines, R.E. Lisle, R.W. Shafer, and W.W. Wilkerson, eds. Reno, Nevada: Geological Society of Nevada. pp. 913–934. 1991.

Poole, F.G. "Flysch Deposits of the Antler Foreland Basin, Western United States." *Tectonics and Sedimentation*. W.R. Dickinson, ed. Society of Economic Paleontologists and Mineralogists Special Publication 22. Tulsa, Oklahoma: SEPM. pp. 58–82. 1974.

Poole, F.G., J.H. Stewart, A.R. Palmer, C.A. Sandberg, R.J. Madrid, R.J. Ross, Jr., L.F. Hintze, M.M. Miller, and C.T. Wrucke. "Latest Precambrian to Latest Devonian Time; Development of a Continental Margin." *The Cordilleran Orogen: Conterminous U.S*. The Geology of North America G–3. B.C. Burchfiel, P.W. Lipman, and M.L. Zoback, eds. Boulder, Colorado: Geological Society of America. pp. 9–56. 1992.

Rahe, B., D.A. Ferrill, and A.P. Morris. "Physical Analog Modeling of Pull-Apart Basin Evolution." *Tectonophysics*. Vol. 285. pp. 21–40. 1998.

Ridgway, K., J. Stamatakos, M. Gutenkunst, P. Dubreuilh. Stratigraphic Analysis and Regional Correlation of Oligocene and Early Miocene Strata in the Yucca Mountain Area. CNWRA report. San Antonio, Texas: Center for Nuclear Waste Regulatory Analyses. 2011.

Scott, R.B. "Tectonic Setting of the Yucca Mountain Region, Southwest Nevada." *Geological Society of America Memoir 176*. Boulder, Colorado: Geological Society of America. pp. 251–282. 1990.

Serpa, L. and T.L. Pavlis. "Three-Dimensional Model of the Late Cenozoic History of the Death Valley Region, Southeastern California." *Tectonics*. Vol. 15. pp. 1,113–1,128. 1996.

Sims, D., D.A. Ferrill, and J.A. Stamatakos. "Role of a Ductile Décollement in the Development of Pull-Apart Basins." *Journal of Structural Geology*. Vol. 21. pp. 533–554. 1999.

Snow, J.K. "Mass Balance of Basin and Range Extension as a Tool for Geothermal Exploration." *Transactions of the Geothermal Resources Council.* Vol. 18. pp. 23–30. 1994.

Snow, J.K. and B.P. Wernicke. "Cenozoic Tectonism in the Central Basin and Range: Magnitude, Rate, and Distribution of Upper Crustal Strain." *American Journal of Science*. Vol. 300. pp. 659–719. 2000.

Spivey, K.H., D.A. Ferrill, J.A. Stamatakos, A.P. Morris, R.A. Donelick, and S.R. Young. "Uplift and Cooling History of Bare Mountain, Nevada, From Apatite Fission Track Thermochronology." Geological Society of America Abstracts with Programs. Vol. 27, No. 6, A-389. 1995.

Stamatakos, J., D.A. Ferrill, A.P. Morris. "Age and Timing of Extensional Faulting and Basin Growth at Crater Flat, Nevada." CNWRA report. San Antonio, Texas: Center for Nuclear Waste Regulatory Analyses. 2011.

Stewart, J.H. "Tectonics of the Walker Lane Belt, Western Great Basin: Mesozoic and Cenozoic Deformation in a Zone of Shear." *Metamorphism and Crustal Evolution of the Western U.S*. W.G. Ernst, ed. Englewood, Cliffs, New Jersey: Prentice Hall. Rubey Vol. VII. pp. 684–713, 1988.

Stewart, J.H. "Extensional Tectonics in the Death Valley Area, California: Transport of the Panamint Range Structural Block 80 km Northwestward." *Geology*. Vol. 11. pp. 153–157. 1983.

Tagami, T. and P.B. O'Sullivan. "Fundamentals of Fission-Track Thermochronolgy." *Mineralogy and Geochemistry*. Vol. 58. pp. 19–47. 2005.

Tagami, T. and C. Shimada. "Natural Long-Term Annealing of the Zircon Fission Track System Around a Granitic Pluton." *Journal Geophysical Research*. Vol. 101. pp. 8,245–8,255. 1996.

Tagami, T., A. Carter, and A.J. Hurford. "Natural Long-Term Annealing of Zircon Fission-Track System in Vienna Basin Deep Boreholes: Constraints Upon the Closure Temperature and Partial Annealing Zone." *Chemical Geology*. Isotope Geology Section 130 (1–2). pp. 147–157. 1995.

Tagami, T., H. Ito, and S. Nishimura. "Thermal Annealing Characteristics of Spontaneous Fission Tracks in Zircon." *Chemical Geology*. Isotope Geology Section 80. pp. 159–169. 1990.

Wagner, G.A. and R. Van den Haute. *Fission Track Dating*. Dordrecht, Netherlands: Kluwer Academic Publishers. 1992.

Weiss, S.I. "Hydrothermal Activity, Epithermal Mineralization and Regional Extension in the Southwestern Nevada Volcanic Field." Ph.D. dissertation. University of Nevada at Reno. Reno, Nevada. 212 pp. 1996.

Wernicke, B.P. "Low-Angle Normal Faults and Seismicity." *Journal of Geophysical Research*. Vol. 100. pp. 20,159–20,174. 1995.

Wernicke, B.P. "Cenozoic Extensional Tectonics of the Western Cordillera." *The Cordilleran Orogen, Conterminous U.S*. The Geology of North America. B.C. Burchfiel, P.W. Lipman, and M.L. Zoback, eds. Boulder, Colorado: Geological Society of America. G-3. pp. 553–581. 1992.

Wernicke, B. and G.J. Axen. "On the Role of Isostasy in the Evolution of Normal Fault Systems." *Geology*. Vol. 16. pp. 848–851. 1988.

Wernicke, B.P., R.L. Christiansen, P.C. England, and L.J. Sonder. "Tectonomagmatic Evolution of Cenozoic Extension in the North American Cordillera Continental Extensional Tectonics." M.P. Coward, J.F. Dewey, and P.L. Hancock, eds. London, England: Geological Society Special Publications 28. pp. 203–221. 1987.

Workman, J.B., C.M. Menges, W.R. Page, E.M. Taylor, E.B. Ekren, P.D. Rowley, G.L. Dixon, R.A. Thompson, and L.A. Wright, "Geologic Map of the Death Valley Ground-Water Model Area, Nevada and California." Miscellaneous Field Studies Map MF-2381-A. Denver, Colorado: United States Geologic Survey. 2002.

Wright, L.A. and B.W. Troxel. "Geologic Map of the Central and Northern Funeral Mountains and Adjacent Areas, Death Valley Region, Southern California." United States Geological Survey Miscellaneous Investigations Series I-2305. 1993.

Yamada, R., T. Tagami, S. Nishimura, and H. Ito. "Annealing Kinetics of Fission Tracks in Zircon: An Experimental Study." *Chemical Geology*. Isotopic Geology Section. Vol. 122. pp. 249–258. 1995.

Zaun, P.E. and G.A. Wagner. "Fission Track Stability in Zircons Under Geologic Conditions." *Nuclear Tracks and Radiation Measurements*. Vol. 10. pp. 303–307. 1985.

Zoback, M.L., R.E. Anderson, and G.A. Thompson. "Cainozoic Evolution of the States of Stress and Style of Tectonism in the Basin and Range Province of the Western United States." *Philosophical Transactions of the Royal Society of London*. Vol. A300. pp. 407–434. 1981.

APPENDIX A
APATITE FISSION-TRACK THERMOCHRONOLOGY

APPENDIX A—APATITE FISSION-TRACK THERMOCHRONOLOGY

Apatite fission-track ages were measured by Raymond A. Donelick (analyst RAD) using the external detector method (e.g., Gleadow, 1981). The natural apatite fission tracks were etched in 5.5N HNO_3 for 20.0 ± 0.5 seconds at 21 ± 1 °C [69.8 ± 1.8 °F]. Thermal-neutron irradiations for age measurement were of 1-hour duration in position A-8 of the Texas A&M University nuclear reactor while the reactor was operating at 1 MW power output, yielding a thermal-neutron fluence of approximately 10^{16} neutrons/cm^2. All mica detectors were etched in 48 percent HF at 24 ± 1 °C [75 ± 1.8 °F] for 12.0 ± 0.25 minutes to reveal induced fission tracks for use in determining apatite grain uranium concentrations. Fission-track length distributions were measured for all samples that yielded apatite fission-track ages following procedures Dumitru (1999, and references therein) outlined with the added step Cf-252 irradiation to enhance their measurability (Donelick, 1991). All measurements were made with a binocular microscope in nonpolarized light at 1562.5 × magnification (100 × dry objective, 1.25 × projection tube, 12.5 × oculars). With few exceptions, the apatite grains studied were dominantly fluorine rich as indicated by their small fission-track etch pit diameters (e.g., Burtner, et al., 1994; Carlson, et al., 1999). The closure temperature for small etch pit, fluorine-rich apatite fission tracks is approximately 130–146 °C [266–295 °F] {cooling rate of 100 °C/my [180 °F/my]; Ketcham, et al. (1999)}.

The apatite fission-track ages reported in this paper include remeasurements performed using grain mounts from some samples reported on earlier (Ferrill, et al., 1996; Spivey, et al., 1995). In our reanalysis, images of all apatite grains were recorded on videotape. The videotapes were then reviewed in detail (for every apatite grain dated) while tracks were simultaneously counted on the mica detector. This procedure ensured proper counting of the mica detector. In addition, we re-irradiated all of the original grain mounts during a single neutron irradiation session and the remeasurements were performed within a 3-week period. The zeta calibration (Hurford and Green, 1983) factor used to calculate the fission-track ages for the reanalyses was determined using only age calibration standards irradiated simultaneously with the samples in this study. Parameter Dpar (Carlson, et al., 1999; Donelick, et al., 2005) was measured for each apatite grain dated, and the mean value of the dated grains for each sample is reported in Table 4-1.

References:

Burtner, R.L., A. Nigrini, and R.A. Donelick. "Thermochronology of the Lower Cretaceous Source Rocks in the Idaho-Wyoming Thrust Belt." *American Association of Petroleum Geologists Bulletin*. Vol. 78. pp. 1,613–1,636. 1994.

Carlson, W.D., R.A. Donelick, and R.A. Ketcham. "Variability of Apatite Fission-Track Annealing Kinetics: I. Experimental Results." *American Mineralogist*. Vol. 84. pp. 1,213–1,223. 1999.

Donelick, R.A., P.B. O'Sullivan, and R.A. Ketcham. "Apatite Fission-Track Analysis." *Mineralogy and Geochemistry*. Vol. 58. pp. 49–94. 2005.

Donelick, R.A. "Crystallographic Orientation Dependence of Mean Etchable Fission Track Length in Apatite: An Empirical Model and Experimental Observations." *American Mineralogist*. Vol. 76. pp. 83–91. 1991.

Dumitru, T.A. “Fission-Track Geochronology in Quaternary Geochronology; Applications in Quaternary Geology and Paleoseismology, Volume 1.” J.S. Noller, J.M. Sowers, and W.R. Lettis, eds. Washington, DC: American Geophysical Union, Geophysical Monograph Series. 1999.

Ferrill, D.A., G.L. Stirewalt, D.B. Henderson, J.A. Stamatakos, K.H. Spivey, and B.P. Wernicke. NUREG/CR–6401, “Faulting in the Yucca Mountain Region, Critical Review and Analyses of Tectonic Data from the Central Basin and Range.” Washington, DC: U.S. Nuclear Regulatory Commission. 1996.

Gleadow, A.J.W. “Fission Track Dating Methods: What Are the Real Alternatives?” *Nuclear Tracks*. Vol. 5. pp. 3–14. 1981.

Hurford, A.J. and P.F. Green. “The Zeta Calibration of Fission Track Dating.” *Isotope Geosciences*. Vol. 1. pp. 285–317. 1983.

Ketcham, R.A., R.A. Donelick, and W.D. Carlson. “Variability of Apatite Fission-Track Annealing Kinetics: III. Extrapolation to Geological Time Scales.” *American Mineralogist*. Vol. 84. pp. 1,235–1,255. 1999.

Spivey, K.H., D.A. Ferrill, J.A. Stamatakos, A.P. Morris, R.A. Donelick, and S.R. Young. “Uplift and Cooling History of Bare Mountain, Nevada, From Apatite Fission Track Thermochronology.” Geological Society of America Abstracts with Programs. Vol. 27, No. 6, A-389. 1995.

APPENDIX B
ZIRCON FISSION-TRACK THERMOCHRONOLOGY

APPENDIX B—ZIRCON FISSION-TRACK THERMOCHRONOLOGY

Zircon grains from 16 samples were analyzed using zircon fission-track thermochronology techniques (e.g., Wagner and Van den Haute, 1992). Eleven of the zircon fission-track age analyses were performed at University of California at Santa Barbara by Ann E. Blythe (analyst AEB), and 5 were performed by analyst RAD. All analyses were performed using the external detector method (e.g., Gleadow, 1981). The natural zircon fission tracks were etched in an eutectic melt of KOH–NaOH at 220 °C [428 °F] for 18–24 hours, the duration being optimized for each sample. Thermal-neutron irradiations were performed at the Cornell University nuclear reactor (results for analyst AEB) or at Texas A&M University (results for analyst RAD); the duration position, duration, and reactor power levels were optimized to provide thermal-neutron fluences of approximately 10^{15} neutrons/cm^2. All mica detectors were etched in 48 percent HF at 18 ± 1 °C [64.4 ± 1.8 °F] for 30.0 ± 0.25 minutes (analyst AEB) or 24 ± 1 °C [75.2 ± 1.8 °F] for 12.0 ± 0.25 minutes (analyst RAD) to reveal induced fission tracks for use in determining zircon grain uranium concentrations. All measurements were made with a binocular microscope in unpolarized light at 1,250 × magnification (100 × dry objective, 1.25 × projection tube, 10.0 × oculars; analyst AEB) or 1,562.5 × magnification (100 × dry objective, 1.25 × projection tube, 12.5 × oculars; analyst RAD). The thermal annealing characteristics of zircon fission tracks are not as well constrained as for apatite fission tracks. In this study, we consider the zircon fission-track data in terms of a zircon partial annealing zone of 230 to 330 °C [446 to 626 °F] and a closure temperature of approximately 250 °C [482 °F] {cooling rate of 10 °C/my [18 °F/my]; Tagami and Shimada, 1996; Foster, et al., 1993)}.

References:

Foster, D.A., A.J. Gleadow, S.J. Reynolds, and P.G. Fitzgerald. "Denudation of Metamorphic Core Complexes and the Reconstruction of the Transition Zone, West Central Arizona: Constraints From Apatite Fission Track Thermochronology." *Journal of Geophysical Research*. Vol. 98, B2. pp. 2,167–2,185. 1993.

Gleadow, A.J.W. "Fission Track Dating Methods: What Are the Real Alternatives?" *Nuclear Tracks*. Vol. 5. pp. 3–14. 1981.

Tagami, T. and C. Shimada. "Natural Long-Term Annealing of the Zircon Fission Track System Around a Granitic Pluton." *Journal Geophysical Research*. Vol. 101. pp. 8,245–8,255. 1996.

Wagner, G.A. and R. Van den Haute. *Fission Track Dating*. Dordrecht, Netherlands: Kluwer Academic Publishers. 1992.